JYVÄSKYLÄ STUDIES IN COMPUTING

15

Kari Saarinen

Near Infra-Red Measurement Based Control System for Thermo-Mechanical Refiners

UNIVERSITY OF JYVÄSKYLÄ

JYVÄSKYLÄ 2001

JYVÄSKYLÄ STUDIES IN COMPUTING 15

Kari Saarinen

Near Infra-Red Measurement Based Control System for Thermo-Mechanical Refiners

Esitetään Jyväskylän yliopiston informaatioteknologian tiedekunnan suostumuksella
julkisesti tarkastettavaksi yliopiston Agora rakennuksessa (Ag Aud. 2)
joulukuun 20. päivänä 2001 kello 12.

Academic dissertation to be publicly discussed, by permission of
the Faculty of Information Technology of the University of Jyväskylä,
in the Building Agora, Ag Aud. 2, on December 20, 2001 at 12 o´clock noon.

UNIVERSITY OF JYVÄSKYLÄ

JYVÄSKYLÄ 2001

Near Infra-Red Measurement Based Control System for Thermo-Mechanical Refiners

JYVÄSKYLÄ STUDIES IN COMPUTING 15

Kari Saarinen

Near Infra-Red Measurement Based Control System for Thermo-Mechanical Refiners

UNIVERSITY OF JYVÄSKYLÄ

JYVÄSKYLÄ 2001

Editors
Tommi Kärkkäinen
Department of Mathematical Information Technology, University of Jyväskylä
Olli Ahonen and Marja-Leena Tynkkynen
Publishing Unit, University Library of Jyväskylä

URN:ISBN:978-951-39-9820-2
ISBN 978-951-39-9820-2 (PDF)
ISSN 1456-5390

Jyväskylän yliopisto, 2023

ISBN 951-39-1115-2
ISSN 1456-5390

Jyväskylä University Printing House, Jyväskylä and
ER-Paino Ky, Lievestuore 2001

ABSTRACT

Saarinen, Kari
Near Infra-Red Measurement Based Control System for Thermo-Mechanical Refiners
Jyväskylä: University of Jyväskylä, 2001, 84 p. (+included articles)
(Jyväskylä Studies in Computing
ISSN 1456-5390; 15)
ISBN 951-39-1115-2
Finnish summary
Diss.

Pulp quality and energy economics are the key issues in any thermomechanical pulping (TMP) plant. The control in TMP plants is affected by two different types of disturbances: the slow wearing of refiner plates and the faster variations in raw material characteristics. Both these have a great effect on pulp quality and the process economy if not properly controlled.

Nowadays pulp properties such as freeness, fibre length distribution, shives, coarseness and even average cell-wall thickness can be measured directly from a pulp sample, but even today there are no methods available to measure production rate or chip moisture accurately enough. The feed-back control systems that are based on pulp property measurements after latency chest can only partially solve the control problem for two reasons: it is not possible to compensate raw material variations that are faster than twenty minutes and due to the multivariable non-stationary connection between raw material variations and pulp properties it is very difficult to select the right control action.

The objective of this thesis was to solve TMP control problems by developing calibration models and methods for the near infra-red (NIR) measurement unit to measure consistency and properties of pulp and a control system to compensate raw material variations. The term consistency is used for traditional reasons and is related to the moisture of pulp.

We have developed a totally new control system to solve raw material variation problems. It is based on consistency measurements and an adaptive control system that manipulates the dilution water flow and the speed of the chip feeder. Variations in specific energy and refining intensity where reduced significantly and are the two most important state variables of the refiner with which to predict pulp quality. The benefits obtained is improved pulp quality, energy savings, increased line availability and production. Freeness, fibrelength, tear and tensile index, variations have decreased up to 80%.

We have shown in this thesis by statistical methods that in addition to the consistency measurement, it is possible to measure with the NIR-technique other pulp properties such as freeness, size distributions, and tensile index. Due to the analyser being mounted directly in the blow line just after the refiner, there is practically no measurement delay. Pulp quality is mainly defined by the

operation of the first stage refiner. The measurement of pulp properties after the first refining stage gives a possibility to develop a new type of fast quality control system that was not possible before.

The main reason for the difficulties to find a good calibration model for the NIR-analyser is the lack of a theoretical model for light scattering by collections of particles, which have varying shapes and surface appearances.

We have begun our theoretical model building by developing a light scattering model for wood fibre, which is the most important particle in pulp. We have modelled the irregular overall shape and the cell-wall thickness of wood fibre using state-of-the-art statistical methods.

Based on the theoretical calculations we are claiming that when we are measuring pulp quality by the NIR technique, we are mostly defining the shape parameters of the average pulp particle, and not so much by their chemical composition.

The agreement with theoretical and experimental results are very good and allows us to use the developed method in solving practical measurement problems. The on going development work will ultimately lead to a significant reduction of calibration samples.

Author's address

Kari Saarinen
ABB Corporate Research Oy
Vaasa, Finland
kari.saarinen @fi.abb.com

Supervisor

Professor Pekka Neittaanmäki
University of Jyväskylä, Finland

Reviewers

Prof. Josu Takala
University of Vaasa, Finland

Docent Heikki Haario
Lappeenranta Univeristy of Technology, Finland

Opponent

Prof. Heikki Koivo
Helsinki Unversity of Technology, Finland

ACKNOWLEDGEMENTS

I would like to take this opportunity to express my sincere gratitude to Prof. Pekka Neittaanmäki for his guidance and continuous support throughout my research. I am grateful to Prof. Josu Takala and Docent Heikki Haario for reviewing the manuscript and giving supporting feedback. I would also like to thank Dr. Kari Muinonen for fruitful co-operation, Dr. Christian Sasse and Mr. Markku Lahtela for their assistance in measurements. Mr. Gary Littler deserves special thanks for his linguistic comments.

This work was financially supported by the Academy of Finland, National Technology Agency (TEKES), ABB Corporate Research Oy, and COMAS Graduate School of University of Jyväskylä.

Finally, I want to express my appreciation to my wife Margit, to my children Viljami and Paula for their patience and understanding.

CONTENTS

ABSTRACT

1 INTRODUCTION 9
2 OBJECTIVES AND STRUCTURE OF THE STUDY 11
3 THERMO MECHANICAL PULPING PROCESS 13
3.1 From chips to pulp – the refining process 15
3.1.1 Theories of refining 17
3.1.2 Refiner motor load 18
3.1.3 Fibre separation and fibre development 20
3.2 Pulp characterization 21
3.2.1 Characterization of the wood fibre 21
3.2.2 Properties of fibre network and handsheets 24
3.3 Control of the refining process 26
4 NIR -TECHNIQUE 28
4.1 Calibration problem 29
4.2 Data pre-treatment 31
4.3 Calculation of calibration parameters 32
4.4 Chemometric tools 32
4.5 Validation 34
4.6 Optimal modelling complexity 36
4.7 Detection of the outliers 36
5 CONSISTENCY MEASUREMENT BASED CONTROL SYSTEM 38
5.1 Consistency measurement 40
5.2 Adaptive consistency control 42
5.2.1 Process-model 43
5.2.2 On-line identification 44
5.3 Quality control 46
5.4 Results of field tests 48
6 CHARACTERIZATION OF TMP PULP BY NEAR INFRA-RED MEASUREMENT 49
6.1 Statistical models 50
6.1.1 Tests in mill I 50
6.1.2 Tests in mill II 57
6.2 Considerations based on physical theories 59
6.2.1 General aspects 60
6.2.2 Gaussian random wood fibre model 62
6.2.3 Analytical calculations 63
6.2.4 Geometric optics approximation 69
7 CONCLUSIONS 75

REFERENCES 77
YHTEENVETO (FINNISH SUMMARY) 84

LIST OF ORIGINAL PUBLICATIONS

I Saarinen K., Application of Adaptive Model Predictive Consistency Control in TMP Mill. Proceedings of the fifth European Conference in Mathematics in Industry (ECMI) conference, Lahti 1990. Heiliö M., ed. Kluwer Academic Publisher, Dordrecht (1990). 335-339.

II Hill J., Saarinen K., Stenros R, On the Control of Chip Refining Systems, Pulp & Paper Canada 94:6 (1993). T 161- T 165.

III Evans, R., Sutinen, R., and Saarinen, K., Refiner control effectively accomplished through adaptive control. Pulp & Paper Canada 96:5(1995). T 163-T 166.

IV Evans R., Saarinen K., Sutinen R., Developments in Sensors and Control Strategies for Refiners. CPPA 78th Annual Meeting, Montreal (1992).

V Sutinen R., Saarinen K., A Novel Control System for Refiners in TMP Plants. SPCI, MILANO (1992).

VI Leiviskä K., Sutinen R., Saarinen K., Optimal Quality Control of TMP Plants. Preprint International Mechanical Pulping Conference, Oslo (1993)
https://www.researchgate.net/publication/306943481_Optimal_quality_control_of_TMP-plants

VII Saarinen K. Method and apparatus for determination of refiner mechanical pulp properties. United States Patent 5 491 340 (1996).
https://patents.google.com/patent/US5491340

VIII Muinonen K. and Saarinen K., Ray optics approximation for Gausian andom cylinders. Journal of Quantitative Spectroscopy and Radiative transfer 64(2000) 201-218.
https://doi.org/10.1016/S0022-4073(98)00147-2

IX Saarinen K. and Muinonen K., Light Scattering by wood fibres. Applied optics 40(28), (2001) 5064-5077.
https://doi.org/10.1364/AO.40.005064

1 INTRODUCTION

Wood fibre is the basic raw material in paper making. In the tree, fibres are connected tightly to make a strong supporting trunk. During paper production these fibres have to be separated in a controlled way and prosessed further into the appropriate form. There are two basic methods to separate fibres: chemical and mechanical pulping, and their combinations. In thermo mechanical pulping (TMP) wood chips are fed between rotating refiner plates, where lignin, the intermediate agent of the fibres, is plastized by water, heat and repeated mechanical action so that the fibres can be ripped.

The control in TMP plant is affected by two different types of disturbances: the slow wearing of refiner plates and the faster variations in raw material characteristics. Both of these variations have a great effect on pulp quality and the process economy if they are not properly controlled.

Control of the chip refining process is one of the most challenging problems in the paper industry for the following reasons:

- variations in chip density and moisture content are the source of many disturbances in the refiner operation and are very difficult to measure on-line
- chip refining is non-linear, highly coupled multivariable process in which the dynamics depends on plate conditions
- relationships between refiner state variables and pulp quality is complex and non-stationary.

Single loop control strategies, which manipulates dilution water, speed of the chip feeder, or plate gap according to refining power, have been applied to this process but because of the process characteristics, all have only limited success.

Near infra-red measurements with multivariate calibration methods is one of the fastest growing analytical techniques in pulp and paper mill applications. The disadvantage of the NIR-technique is that every analyser must be calibrated against laboratory samples during each installation. Except for consistency measurements, the required number of calibration samples is quite

high in order to achieve a robust and accurate measurement. Usually trial and error is the only method available to find out the right calibration model.

Understanding the light scattering properties of paper particles, especially of wood fibres, plays an important role when new optical or spectroscopical sensors and their calibration models are developed. When light scattering characteristics are studied a shape model for particle is always needed. In the recent theoretical studies, the stochastic shape of the hollow cylindrical like wood fibre have been modelled by an infinite solid circular cylinder, by a sphere or by a plate. It is clear, that with these models, it is not possible to study how the changes for example in the shape or in the cell-wall thickness of the fibre affect the light scattering characteristics. Also experimental studies have shown that scattering by apparently cylindrical biological objects produces patterns that could not be predicted by the circular cylinder scattering theory.

2 OBJECTIVES AND STRUCTURE OF THE STUDY

The objective of this study was to develop measurements and control systems for thermo-mechanical refiners. This thesis was carried out gradually by solving the oncoming problems.

Development steps.

1. Developing a multivariate calibration model and method for near infrared consistency analyser.
2. Developing a consistency measurement based control system that stabilises the mass-flows
3. Developing a quality control system for the thermomechanical pulp mill of Papeterie du Golbey.
4. Developing a multivariate calibration model and method for near infrared analyser to measure pulp properties.
5. Developing simulation tools to understand the light scattering by wood fibres.

This thesis is based on nine publications and unpublished results presented in Chapter 6.

I Saarinen K., Application of Adaptive Model Predictive Consistency Control in TMP Mill. Proceedings of the fifth European Conference in Mathematics in Industry (ECMI) conference, Lahti 1990. Heiliö M., ed. Kluwer Academic Publisher, Dordrecht (1990). 335-339.

II Hill J., Saarinen K., Stenros R, On the Control of Chip Refining Systems, Pulp & Paper Canada 94:6 (1993). T 161- T 165.

III Evans, R., Sutinen, R., and Saarinen, K., Refiner control effectively accomplished through adaptive control. Pulp & Paper Canada 96:5(1995). T 163-T 166.

IV Evans R., Saarinen K., Sutinen R., Developments in Sensors and Control Strategies for Refiners. CPPA 78th Annual Meeting, Montreal (1992).

V Sutinen R., Saarinen K., A Novel Control System for Refiners in TMP Plants. SPCI, MILANO (1992).
VI Leiviskä K., Sutinen R., Saarinen K., Optimal Quality Control of TMP Plants. Preprint International Mechanical Pulping Conference, Oslo (1993)
VII Saarinen K. Method and apparatus for determination of refiner mechanical pulp properties. United States Patent 5 491 340 (1996).
VIII Muinonen K. and Saarinen K., Ray optics approximation for Gausian andom cylinders. Journal of Quantitative Spectroscopy and Radiative transfer 64(2000) 201-218.
IX Saarinen K. and Muinonen K., Light Scattering by wood fibres. Applied optics 40(28), (2001) 5064-5077.

The role of marketing manager R. Evans and sales manager R. Stenros was to act as contacts and introduce marketing material into the papers. Mr. Evans presented the papers III and IV and thus his name is first on the list.

The introduction part is organised as follows. In Chapter 3 we introduce the refining process, its measurements and previous control systems. In Chapter 4 we introduce NIR technique. In Chapter 5 we describe the new consistency measurement based control system based on publications [I], [II], [III], [IV], [V] and [VI]. In Chapter 6 we consider pulp characterization by NIR technique empirically and theoretically. Empirical results are based on publications [VII] and tests with new analyser in TMP mills. The new theoretical calculations for single particle albedos, asymmetry parameters and phase functions are based on wood fibre models published in [VIII], [IX] and analytical solution for layered circular cylinder. We also give comparisons between analytical and geometric optics solutions for an infinite two-layer circular cylinder. We close with conclusions in Chapter 7.

3 THERMO MECHANICAL PULPING PROCESS

The history of stone groundwood pulping begins in the early 1800s and it has been the dominant method of producing mechanical pulp until the late 1970s. The refining process was developed during 1948-1956 by Bauer Bros. [4]. The Thermo Mechanical Pulping process (TMP) was developed about 10 years later and has become the most important mechanical pulping method. In Finland the first TMP-line was started in 1975. There are several reasons for the continuously increasing capacity of producing TMP pulp:

Compared to chemical pulping:

- production costs are lower
- higher yield 95-98% (only 40 –45 % in chemical pulping)
- process equipment is cheaper
- no chemicals are used

Compared to grinding:

- possibility to use saw mill residual as raw material
- better strength properties
- less staff needed for handling the process

The disadvantages are high energy consumption, finite brightness of the paper and tendency of turning yellow afterwards.

TMP pulp is the main raw material for newsprint. Since the 1970s different wood containing high-quality printing grades (SC, LWC, etc.) has become a major and very demanding end use for mechanical pulps. Their excellent properties for this purpose are largely due to the fines material in pulp. TMP pulp fines consists of a wide range of particles: pieces of fibres, large cell-wall fragments, fibrills, and ribbon like material. Due to this special characteristic, TMP pulp fines can simultaneously improve the tensile strength, the smoothness and the light scattering properties of paper. The replacement of

chemical pulp by TMP pulp is limited by the quality of the fibre attainable by TMP.

There are different versions of the refiner mechanical pulping processes:

- **RMP**-process or **original refiner mechanical pulping process**, in which the unheated wood chips are refined in an open refiner
- **PRMP**-process or **pressure refiner mechanical pulping process**, in which the unheated chips are refined in the pressurized refiner.
- **TMP**-process or **termomechanical pulping process**, in which the chips warmed by steam are refined in a pressurized refiner.
- **CMP-CTMP** -processes or **chemi-mechanical pulping and chemi-thermochemical pulping processes**, in which different chemicals are used in addition to heat and mechanical work to improve the brightness of pulp and reduce energy consumption

In addition to the grouping above there may be considerable variations between the processes of the same type depending on the supplier of the process equipment. The overall flow diagram of the TMP process is shown in FIGURE 1.

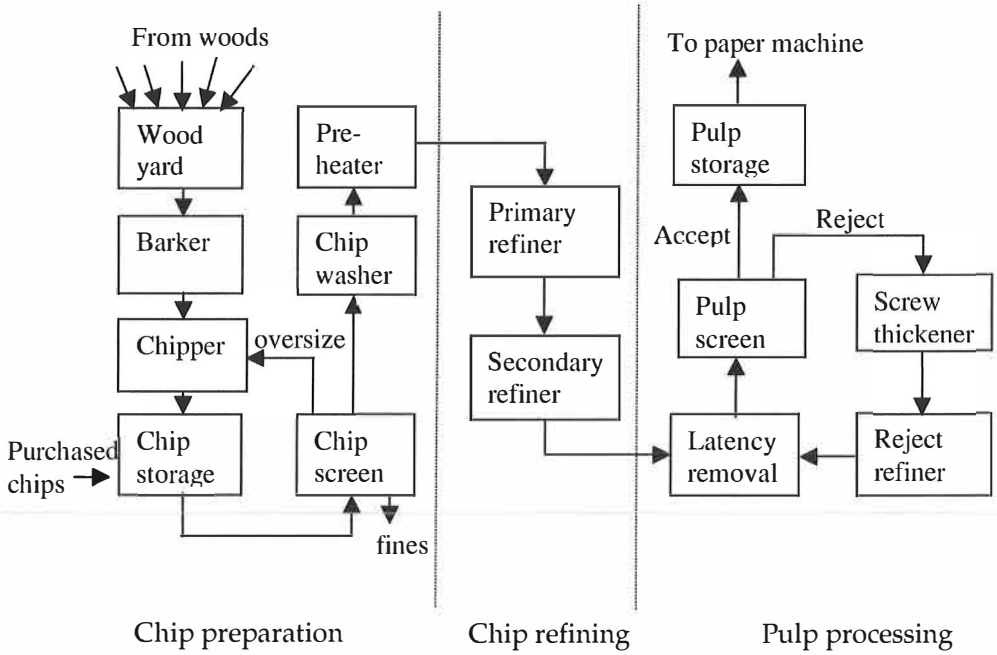

FIGURE 1. Flow diagram of a typical TMP process.

Mechanical refiners use either whole tree chips or residual chips as raw material. Whole tree chips are usully made on site from roundwood. Residual chips are usually purchased from saw mills or plywood mills and they are

made from wood residues. The quality of the chips is important and therefore they are screened and washed. When screening, really large and really small chips are removed from the chip flow. During washing sand, scrap and other foreign material that can cause damage to the refiner are removed from the chips. The warm washing water also defrosts any possible ice on the chippings.

In the pressurized preheater the chips are warmed by steam so that the lignin is softened. This promotes the fibre separation and increases the strength properties of the pulp.

The actual chip refining is usually carried out in two stages. The first stage is pressurized and warmed with steam. The high temperature during refining softens the fibres and allows their separation with minimal cutting and fines compared to RMP or groundwood pulping. The steam produced by the refiner blows the pulp to the second stage of refining, which can be either pressurized or not.

After refining the latency in pulp is removed by diluting with warm water and blending heavily in the latency chest from 15 to 60 minutes. Due to this, the bonding ability of the pulp is better, fibres are more flexible and the pulp is ready for screening, where pulp is separated from shives (i.e. small bundles of fibres). The shives are thickened, refined in the reject refiner and returned to the main pulp flow.

The economy of the process is improved by heat recovery units in both stages. The heat from the steam may be used for example by the paper machine or in local district heating networks.

3.1 From chips to pulp – the refining process

Chip refining is a very fast process. Huge amounts of energy is used in a small volume between the discoidal refiner plates during about one second of the residence time of the pulp. The rated power of the refiner motor that rotates the plates can be as large as 25 MW. The diameter of the refiner disc can be close to two meters and is covered with plate segments, in which radially directed grooves and bars alternate. The number and shape of the bars and grooves varies in different plate sections.

There are various types of refiners. The double-disc refiner has two refining zones on both sides of a disc, that rotates between two static discs, while the single-disc refiner has one refining zone between a rotating disc and a static disc. There can also be two refining zones in a single disc refiner. The Sunds Defibrator RGB CD-70 refiner has a plane and a conical refining zone, with which the gaps can be controlled independently.

The space between the refiner plates, the plate gap, is the main operation variable, and is controlled either by a hydraulic or mechanical loading system. The distance between the plates is typically in the range of 0.1 to 1.0 mm depending on the refining stage and due to the slightly tapered shape of the gap, it is smallest at the end of the refining zone.

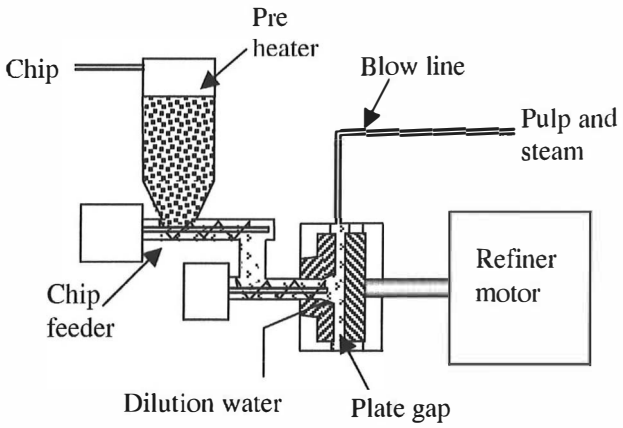

FIGURE 2. Simplified diagram of a first stage refiner.

The production rate i.e. dry-wood material flow $\dot{m}_f$ is controlled by changing the speed of the chip feeder. Together with dry-wood material, three water flows from different sources are flowing into the refiner: water in chips $\dot{m}_{cw}$, dilution water $\dot{m}_{dw}$ and seal water $\dot{m}_{sw}$. The ratio of the water and dry-wood material entering into the refining zone is a very important variable in chip refining. For traditional reasons the consistency value is used as a unit of measurement, although the moisture content is used when the amount of water in chips is described. The so called inlet consistency is used as a unit of measurement to describe the ratio between the dry-wood material and water just before the refining zone

$$c_i = \frac{\dot{m}_f}{\dot{m}_f + \dot{m}_w}, \quad \dot{m}_w = \dot{m}_{cw} + \dot{m}_{dw} + \dot{m}_{sw}. \tag{1}$$

In the refining zone the consistency changes due to the conversion of water to steam. The consistency of pulp after the refining zone is called outlet consistency or just consistency and it is defined

$$c_o = \frac{\dot{m}_f}{\dot{m}_f + \dot{m}_{pw}}, \tag{2}$$

where $\dot{m}_{pw}$ is water that flows within pulp. Quite often consistensies are reported in percentage units i.e. multiplied by 100%.

3.1.1 Refining theories

Various empirical and mechanistic models have been developed in order to understand the connection between refiner state variables and pulp quality, and also to be able to develop the refiner itself.

The most important state variable of the refining process is specific energy E, which descibes how much energy is used per produced pulp

$$E = \frac{W}{\dot{m}_f}, \tag{3}$$

where W is refiner motor load (also called refining power).

It is commonly known and it has been repeatedly observed (not later than 1972 [57]) that there is strong correlation between pulp quality and specific energy. In addition to specific energy Strand and Hartler [91] used in their study 1985 relative residence time, and plate vibration as independent variables in polynomial models to predict pulp quality. Relative residence time was estimated as a ratio of refiner volume and volumetric flow rate.

Due to the fact that a lot of steam is generated in the refiner, steam flow models have been developed to aid in the development of refiners [58],[66],[68].

Pulp that flows through the refining zone has different velocities than steam. Miles et al. [59],[60],[61],[62] have developed a model for pulp flows that can explain the effects of specific energy and consistency on refining process and pulp quality. In addition to specific energy they introduce a state variable called refining intensity.

If the specific energy is held constant, the residence time controls the the average amount of energy transferred per impact of the bar: this average specific energy per impact is the refining intensity. The quality of pulp will depend not only on the specific energy applied, but also on the intensity with which it is applied.

The refining intensity is approximately

$$e = \frac{E}{\bar{n}}, \tag{4}$$

where $\bar{n}$ is the approximation for the average number of bar impacts

$$\bar{n} = \bar{N} a_1 \omega \frac{(r_1 + r_2)}{2} \tau, \tag{5}$$

and

N = average number of bars per unit length or arc
ω = rotation speed of the plate
a_1 = 1 for a single-disc refiner, 2 for a double-disc refiner.

Miles [62] gave also a simplified formula for residence time

$$\tau = \frac{\mu_r}{\mu_t \omega^3} \frac{a_2 L c_i E}{L(r_2^2 - r_1^2) + r_1^2 c_i E} \left[\ln\left(\frac{r_2}{r_1}\right) - \frac{1}{2} \ln\left(\frac{L - c_i E}{L}\right) \right], \quad (6)$$

where

r_1, r_2 = the inner and outer radii of the refining zone, respectively
μ_r, μ_t = the friction coefficients between the pulp and the refining elements in the radial and tangential directions respectively,
a_2 = 4 for a single-disc refiner, 2 for a double-disc refiner
L = latent heat of steam.

The energy and consistency term in (6) always occur together as a product, thus the refiner can be run at a constant residence time if this product is kept constant. This equivalence does not extend to the refining intencity, because the latter is determined by both residence time and specific energy (4). It has been shown by Miles [62] that the refining intensity is nearly independent of the specific energy if the inlet consistency is kept constant. In other words the refining intensity is mostly defined by the inlet consistency.

According to Miles and May [59]:" The consistency is perhaps the most important variable in the chip refiner because it determines the quality of pulp that can be obtained for a given specific energy."

3.1.2 Refiner motor load

At a constant production rate the refiner motor load determines the specific energy. The model by Miles et al. does not predict the motor load, but it is taken as measured value. The connection between the motor load and operational parameters is complicated and changes with plate condition due to wearing. FIGURE 3 visualizes the experimental relationship between the motor load and plate gap, and between motor load and outlet consistency.

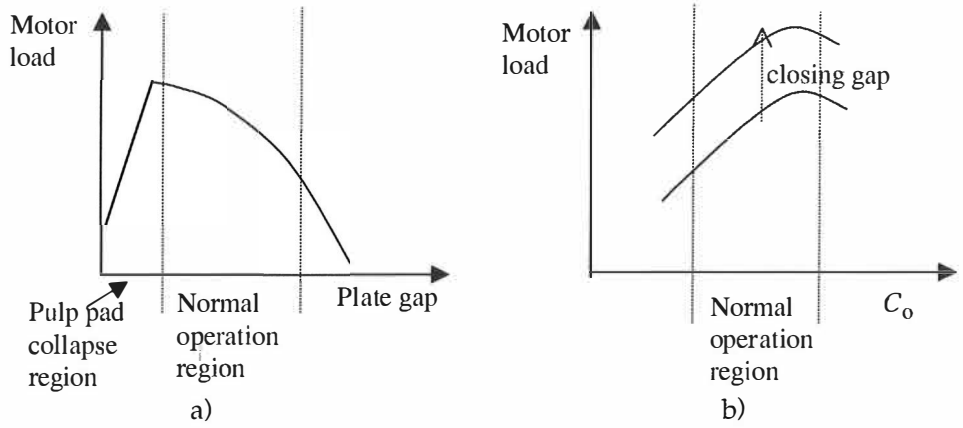

FIGURE 3. Illustrative example of the non-linear relationship between a) plate gap and refiner motor load [17] b) outlet consistency c_o and refiner motor load [79] and [II].

The refiner motor load increases as the plate gap closes until a maximum point is reached. After this point further plate gap glosure will cause the pressure between the plates to drop suddenly and the plates plates will make contact with each other (plate clash) resulting in a production brake and excessive wear on the plates. According to Miles and May [59] plate gap controls the steam velocity. Closing the gap will increase the speed of blow-back steam, which will after certain point cause feeding problems. The shape and the maximum point of the motor load – gap relation curve depends also on production rate, inlet consistency and plate condition.

Assuming that the latent heat of steam L is independent of pressure, the connection between inlet and outlet consistencies can be approximated by the formula [59]

$$c_o = \frac{c_i}{1 - c_i E / L}. \tag{7}$$

This shows that, at a given production rate the inlet consistency has double effect on outlet consistency. Firstly, it will change outlet consistency directly according to equation (7) Secondly, decreasing the inlet consistency will increase the motor load, which will increase the specific energy E. Likewise when closing the cap, the motor load will increase with decreasing inlet consistensy until a maximum point is reached. After that point the motor load and outlet consistency will decrease and the refiner becomes unstable. The consistency at the maximum point is higher for larger refiners.

An even consistency of 20 – 30 % is ideal for primary refining and is the most important operating variable; a consistency which is too low will result in

a refining intensity which is too high. This can cause fibre damage and lots of short fibres. While much higher consistencies cause the refiner to plug.

3.1.3 Fiber separation and fiber development

The refining process may be divided into two concurrent stages [39]:

- fibre separation stage and
- fibre development stage.

In the fibre separation stage, also called defibration stage, the chips are broken down into shives and long intact fibres. This stage requires relatively little energy [37].
Fibre development is a term used in mechanical pulping to indicate the changes in the fibre properties which occur during refining and are important in determining the paper making potential of pulp. Karnis [39] presented two theories of fibre development:

- The communition theory. Part of the long fibres are broken into shorter fibres and fines
- The peeling-off mechanisms the fibre wall material is first delaminated and eventually peeled-off to form short fibres and fines.

According to Karnis [39] the peeling-off mechanism in which the fibre development proceeds by delamination and eventually peeling-off the P and S_1 layers, exposing the S_2 layer, is more probable. He found the S_2 layer to be occasionally disrupted. Other studies support the peeling-off mechanism by showing that a major part of the fibre development consists of a gradual reduction of cell-wall thickness.

Johnsen et. al. [33] studied the surface material and the cross sections of TMP fibres by scanning electronic microscope (SEM) method and found that the middle lamella coverage was 13 - 24 % after first the stage refiner dropping to 10 - 15 % after the second stage refiner. They also found continuous cell-wall thickness reduction during the refining process. Reme and Helle [75] reported that the cell-wall thickness decreased linearly with increased specific energy.

Studies about origin, size, shape and chemical composition of fines particles also supports the peeling-off mechanism. The middle lamella - primary wall portion of the wood cell does not have any fibrillar structure and the particles originating from this fraction are small flake-like particles [63]. Luukko and Nurminen [51] found that the effective fibril length and fibrillar content of fines increased with specific energy, suggesting that more fibrillar particles were peeled of the fibre wall. The peeling-off mechanism requires a relatively high amount of energy [88].

3.2 Pulp characterization

The aim of the refining process is to produce pulp with good quality for different end use applications. To be able to develop the quality of the pulp in a controlled way, the mechanism of the refining process and how the control variables effects on the pulp quality have to be understood. Wood fibre and its properties has a major role in the characterisation of pulp.

3.2.1 Characterization of the wood fibre

Wood fibre has a stochastic shape. The fibre diameter, cell-wall thickness, and the fibre length are (practically) lognormally distributed [33], [43], [15], [99]. The cell-wall thickness varies significantly about the fibre axis, often by a factor of two or more. Shape charasteristics and their values are important when the effect of refining is studied.

The internal structure of a wood fibre particle is very complicated. The fibre cell consists mainly of cellulose, hemicelluloses, and lignin. In a simplified picture, the cellulose molecules form long chains that consitute elementary fibrills, micro-fibrills and, finally, greater fibrills and lamellae. These are surrounded by other substances. The cell wall consists of several layers: the middle lamella (M), primary wall (P), outer layer of secondary wall (S_1), middle layer of secondary wall (S_2), inner layer of secondary wall (S_3), and warty layer. The middle lamella is located between the fibres and its function is to bind the fibres together in wood. The hole in the center of the fibre is called lumen. The S_2 layer is generally the thickest one and its effect dominates the overall properties of the fibre. The structure and chemical composition differ for each layer [95].

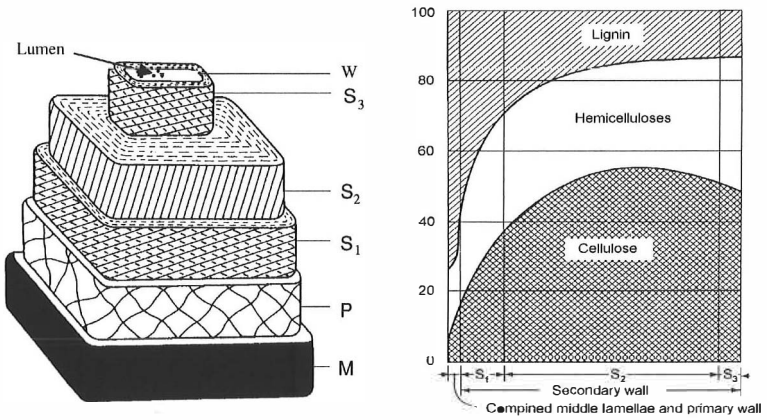

a) b)

FIGURE 4. Schematic of the construction of the cell-wall [32]. a) Cell-wall layers: middle lamella (M), primary wall (P), outer layer of secondary wall (S_1), middle layer of secondary wall (S_2), inner layer of secondary wall (S_3), and warty layer (W). Also the orientation of the fibrils can be seen. b) Distribution of chemical components across the cell-wall.

The measurement of diameter of fibre with stochastic shape is not simple. FIGURE 5 a) shows a cross section of stochastic shaped fibre generated by Gaussian random fibre model (Chapter 6.2.2). Origin is marked with '**x** '. An often used estimate for diameter is, so called Feret diameter D_F, the maximum distance of a pair of points on the fibres outer surface. An other usuall estimate is the orthogonal projection length D_p. There can be a considerable difference between the different diameters. In the example in FIGURE 5 a) D_F = 44 µm, D_p = 39 µm and the diameters calculated from average radius which origin is marked with '**x** in is 35 µm.

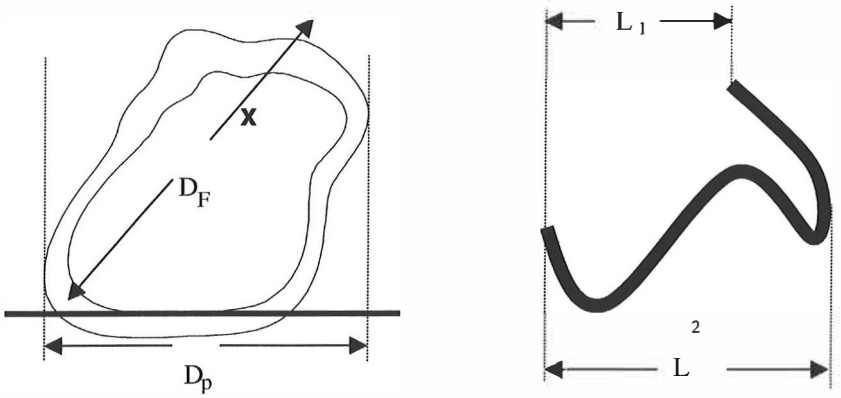

FIGURE 5. Definition of fibre diameters and curl factors. D_F is Feret diameter, D_p is projected diameter. Origin is marked with 'x'.

TABLE 1 shows the average, median, and standard deviation for the cell-wall thickness and diameters (D_F) of a spruce fibre. Cross-sections of the fibres were analysed by scanning electron microscope (SEM) technique [43]. Johnsen et. al. [33] measured TMP fibres and got average 2.66 µm and standard deviation 1.16 µm for cell-wall tickness.

TABLE 1 Cell-wall thickness and fibre width. EW = earlywood, LW= latewood [43]

Property	All	EW	LW
Cell-wall thickness, [µm]			
average	4.8	4.3	7.8
median	4.2	3.9	7.4
standard deviation	2.2	1.8	2.1
Fibre diameter, [µm]			
average	38.8	40.8	26.1
median	36.6	38.6	24.6
standard deviation	14.1	13.8	7.6

Fibre length can be measured microscopically, by classification with screens or by optical scanners. Microscopical measurement is very tedious, that is why automatic measurement devices that use optical methods have been developed. Fibre length can also be analysed using a series of at least four screens of increasingly smaller openings. (TAPPI standard T 233, SCAN-M6:69). Most common instrument is Bauer-McNett type, which is used in laboratories around the world. The deviation between different apparatuses is large, but the repeatability of the single apparatus is acceptable [49].

So called *curl factor* (FIGURE 5 b) is used to characterise the longitudinal shape of the fibre. Jordan et al. [34] gave three different definitions for curl factors

$$C_1 = L_1 / L$$
$$C_2 = L_2 / L$$
$$C_3 = (L / L_2 - 1),$$

where L is the length measured along the mid-line of the fibre. C_3 is the most commonly used.

Modern optical analysers provides estimations for several fibre properties such as average fibre length, fibre length distribution, average fibre width, width distributions, and cell-wall thickness.(e.g. PQM1000 [86], Kajaani FS200 [42]).

Fibre diameter and cell-wall thickness are practically lognormally distributed [33], [43]. In modelling fibre length distribution Dopson [15] and Tornberg et. al. [99] used FS200 intrument and lognormal distributions. Also the distribution of cul factor C_3 has lognormal shape in the Jordan et. al.'s article [34].

3.2.2 Properties of fibre network and handsheets

Handsheet properties (tear index, tensile index, burts index, opacity, bulk, brightness, etc.) are used to predict the properties of paper in actual use. These cannot be measured on-line, thus one has to rely on laboratory tests that take long time to analyse.

Due to the long delay it is impractical to control the pulp quality in the normal operation by measuring handsheet properties. Mills have developed different strategies by measuring other pulp properties that correlates with handsheet properties. Nowadays handsheet properties can also be predicted based on on-line measurement of pulp properties [94].

Forgacs [20] investigated the strength properties and the particle size distributions of refiner mechanical pulp in 1962. He found that the handsheet properties of the mechanical pulp such as burst strength, tear strength, bulk and wet web tensile strength could be predicted for a wide range of SGW pulps on the basis of only two pulp characterization indices:

- The length factor (in short, L factor) characterisizing the fibre length distribution.
- The shape factor (in short, s factor or specific surface) characterizing the degree of the fibre surface development

According to the Stationwala et. al. [88],[89] the Canadian standard freeness (CSF) depends on specific surface of fines in a pulp and fibre flexibility.

Broderic et. al. [7], used latent vector analysis (PLS) to construct models which relate the variations in hand sheet properties to changes in both physical and chemical intrinsic fibre characteristics. They found that the specific surface area and fibre flexibility were the most important factors in the Canadian standard freeness model.

In paper, fibres are held together by hydrogen bonding of the hydroxyl groups of cellulose and hemicelluloses. The carboxylic acid groups of hemicelluloses, also play an important role. Lignin is not able to form hydrogen bonds, thus lignin on fibre surface decreases the strength of the paper [4].

Mohlin showed that [63] the bonding ability of long fibres is related to both fibre flexibility and fibre surface properties. According to Paavilainen [67] cell-wall thickness explained 80% of the paper property variations of strength and printing properties of the sulfate pulp when the cell-wall thickness of the raw material varied between 4 and 9 μm and fibre length between 1.95 and 2.5 mm.

We can conclude that the flexibilty of fibre, specific surface area, average fibre length and lignin coverage are important factors when pulp is characterized.

Karnis has developed a formula for flexibility [39]

$$\text{Flex} = \frac{1}{\kappa \frac{\pi}{64}\left(D_f^4 - D_L^4\right)}, \tag{8}$$

where κ is elastic modulus of the cell-wall, D_f and D_L, the diameters of the fibre and the lumen, respectively. Also a formula for stiffness, which is inversely related to flexibility, has been developed [10]

$$\text{Stiff} = \frac{2}{3}\kappa D_f a_c^3, \tag{9}$$

where a_c is the cell-wall thickness. Equations (8) and (9) show that flexibility and stiffness are very sensitive to changes in cell-wall thickness.

Freeness is a good measure of fibre flexibility and specific surface and so in the other words it is well related to Forgacs' s-factor. So in practice, the quality of refiner pulp can be described quite well with freeness and fibre length distribution.

Due to the fact that freeness and fibrelength distribution are easy to measure and there exist accurate on-line analysers for these as well, quite many mills have adopted this strategy to monitor pulp quality.

3.3 Control of the refining process

The main objectives of controlling the refining process are a stable refiner operation and uniform pulp quality. When the refiner operation is stabilized, it is then possible to optimize the operating set points to give a consistent product with the desired quality charasteristics as well as to use the input energy more efficiently or to increase the production.

The basic refiner control is a measurement problem. The main obstacle to controlling specific energy is that even today the production rate cannot be measured accurately. MacDonald and Guthrie [52] reported an attempt to use the gamma radiation method for chip mass flow measurement. They point out the importance of a moisture mesurement to clarify both the absolute amount of dry wood and the amount of water that chips carrie. Fournier et. al. tried [21] unsuccesfully to measure the chip moisture at the same location, through the plug-screw of the refiner.

The refiner itself senses these disturbances. The average refiner motor loads are typically reduced to prevent accidental overloads due to the disturbances. Various control strategies have been tested to reduce the refiner load variations. Some mills have made the assumption about the dominant disturbance and have manipulated either the dilution water flow [13],[101] or the speed of chip feeder [97],[11] according to the motor load.

Many advanced control algorithms: the self tuning controller [18], neural net-work controller [45], and the dual-adaptive controller [1], have been developed to stabilize refiner motor load by manipulating the plate gap. Although this may limit load fluctuations, it affects the volumetric conditions in the refining zone and will introduce changes in refining intensity therefore in the quality of pulp. Further if a change in the production rate is controlled by maintaining the refiner motor load, the specific energy will change and therefore the quality of pulp.

Nowadays many pulp properties can be measured directly from a pulp sample, taken after latency chest. Advanced single loop freeness controllers have been developed by Cameron et. Al.[8], and by Toivonen and Tamminen [98]. Trials in a two-stage refiner line producing news sprint pulp [93] showed that compared to an uncontrolled trial this type of freenes control could significantly reduce freeness variations, but at the same time variations both in tear and tensile index increased due to the control actions.

The feed-back control systems that are based on pulp property measurements after latency chest can only partially solve the control problem for two reasons: it is not possible to compensate raw material variations that are faster than twenty minutes and due to the multivariable non-stationary connection between raw material variations and pulp properties it is very difficult to select the right control action.

FIGURE 6 sumarises the variables around the first stage refiner. The list is not complete. For example important measurements that affects the

productivity and that are used by modern predictive maintanence systems [100] and related patents [83],[84][85], are not presented.

When implementing the control system the operator interface must be planned carefully, because, if the operators are not willing to use the system, the control has failed, no matter how advanced it is.

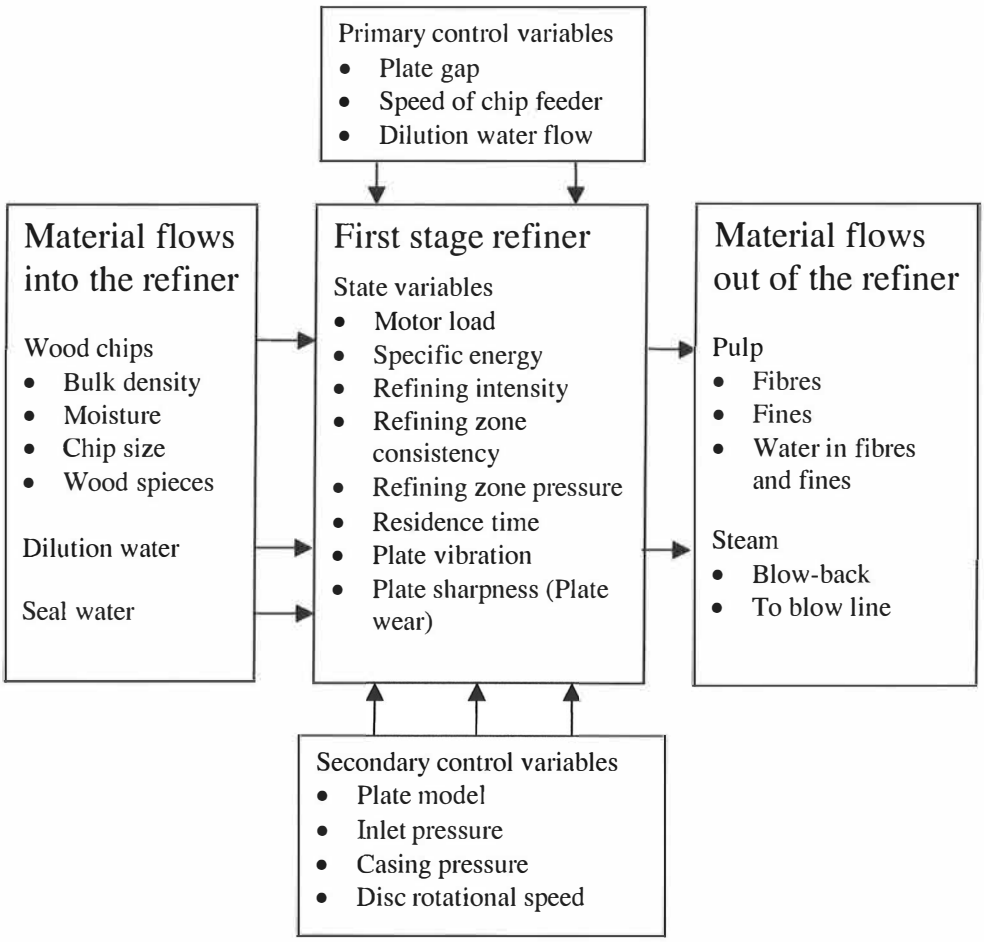

FIGURE 6. Variables of the first stage refiner.

4 NIR -TECHNIQUE

Near-infrared (NIR) spectrometry and multivariate calibration methods – NIR-technique – is a very powerfull tool to measure industrial processes and product quality within many branches of the industry. NIR measurement is fast, non-destructive, cost effective and needs no sample preparation. For these reasons NIR spectroscopy is one of the fastest growing analytical techniques [54].

The NIR-technique is usually used to give information about chemical composition of the measurement object. Molecules, consisting of electrically charged nuclei and electrons, may interact with the oscillating electric and magnetic fields of light and absorb the energy carried by the light. Light in infrared frequencies can generally promote molecules from one vibrational energy level to an other. The absorption peaks in the NIR region originate from the same molecular vibrations that give signals in the infrared region. Each molecule has a unique absorption spectra and thus the measurement of their concentrations is possible.

McClure reviewed the history and measurement technique of NIR spectroscopy [54]. The NIR region was discovered by William Herschel in 1800. The NIR spectrum that starts at 700 nm and ends at 2500 nm can be divided into two regions: Herschel region from 700 – 1100 nm, where silicon detectors can be used, and the region between 1100 and 2500 nm, where lead sulfide detectors are used [54]. Karl Norris was the first to use the NIR spectroscopy to analyse chemically complex solid samples [54].

In the pulp and paper industry the NIR region has been used traditionally when measuring the moisture content of paper ([47] and references therein). The NIR technique has also been used in quantifying hardwood-softwood mixtures, estimating ligning content (Antti [2] and references therein).

4.1 Calibration problem

In pulp and paper mill applications the NIR instrument must always be calibrated against reference values. Calibration means that we want to transform the measurement signals to the desired physical/chemical value readings. In mathematical terms it means that we need a function F, the calibration model, that transforms the future measurement signals $\mathbf{R}_i = [R_{i,1}, R_{i,2}, ..., R_{i,K}]$ (i>N, K is the number of wavelength bands) to desired value readings $\mathbf{v}_i$

$$\mathbf{v}_i = F(\mathbf{R}_i, \mathbf{B}) \tag{1}$$

as accurately as possible. Moreover, we need a method to estimate the unknown coefficients $\mathbf{B}$ using N calibration samples that correspond to the measurement signals $\mathbf{R}_i$ (i≤N). By nature this problem is different than the "curve fitting" -problem, where we want to minimise the error between calculated and reference value when i ≤ N.

When we are solving the calibration problem we are actually seeking a solution to the inverse light scattering problem. At the present stage the calibration models are much more empirical (statistical) models than 'closed' causal ones.

The absorption peaks in NIR-region are broad and difficult to interpret because they are built up by overtones and combination bands. It is difficult to find a single measurement band that can predict the wanted values and on the other hand there can be stong correlation between the measurement bands. In addition, the changes in light scattering charasteristics of the pulp particles can cause overall chances in measured spectra and their shapes.

Due to these problems calibration methods that assume each wavelength have unique information, like the traditional multiple linear regression, can't be used. Some "rank deduction" is needed for calibration.

Present solution to the calibration problem is described in FIGURE 7.

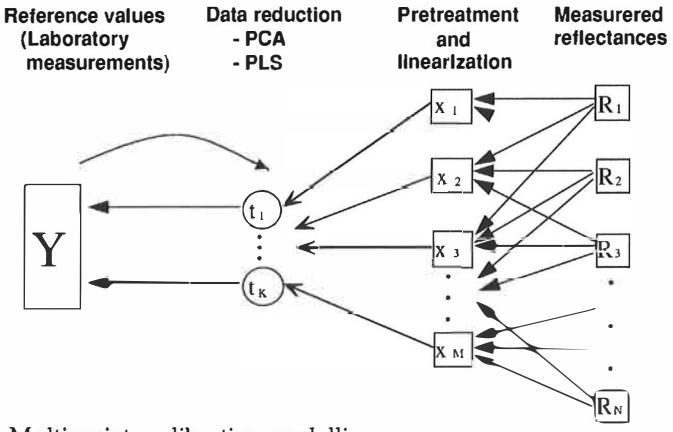

FIGURE 7. Multivariate calibration modelling

Pre-treatment and linearization forms the calibration model. Data reduction methods together with regression techniques such as principal component regression (PCR) and partial least squares (PLS) to latent structure are used to estimate the calibration coefficients. In the following those methods are briefly intoduced. For more detailed information on PLS and PCR we recommed the books by Martens and Naes [53] and Jolliffe [35].

Let N be the number of calibration samples taken from processs and $\mathbf{R}_i$ reflectance spectrum that corresponds to sample i:

Let $\mathbf{v}_i$ be a corresponding vector of quantities of sample i:

$$\left[v_{i,1}, v_{i,2}, v_{i,3}\right] = \left[\text{consistency, freeness, fines}\right].$$

For reliable predictions we need a good calibration model F and a method to estimate the calibration parameters. The simplest calibration model is the linear regression model:

$$\mathbf{v}_i = \mathbf{R}_i\mathbf{B} + e_i \tag{2}$$

where is $\mathbf{B}$ matrix of unknown calibration parameters and e represents the residual. In order to keep notations simple, the matrix $\mathbf{B}$ and $\mathbf{R}_i$ are assumed to include the intercept .

If the linear model (2) is not good enough, it is much more difficult to solve the problem. In most cases good results can be achieved by using pre-treatment of the signals and applying transformation of $\mathbf{R}_i$ variables followed by linear modelling.

After transformations we will have a linear model:

$$\mathbf{v}_i = \mathbf{x}_i\mathbf{B} + e_i, \tag{3}$$

where $\mathbf{x}_i = f(\mathbf{R}_i)$. Again, to keep notations simple we use equation (3) also when no transformations are used. Then the function f is identity mapping.

To be able to select the best calibration model we have to have a method to measure the performances of each models. The most commonly used criterion for model selection is root mean square error of prediction (RMSEP). Before model selection, we must have a method to estimate the calibration parameters.

4.2 Data pre-treatment

Finding the optimal transformation of variables can be extremely complicated. Fortunately in multivariate calibration this may not be needed - a pre-processing that gives a reasonable linearity may be enough, but at the cost of an increased number of calibration parameters.Due to the lack of a physical model, we must often choose data pre-treatment and transformation functions using earlier experience, visual observation, or simply by trial and error method.
A well known example of spectroscopic pre-linearization is the transformation of transmission data into absorbance using function $\log(1/T)$, where T is the measured transmission spectra. This gives us a transformation

$$x_{i,j} = \ln(R_{i,j}). \tag{4}$$

The following tranformation equation is based on Kubelka-Munk theory [46]

$$x_{i,j} = \frac{(1-R_{i,j})^2}{2R_{i,j}} \tag{5}$$

Difference of logarithmic values reads

$$x_{i,j} = \ln(R_{i,j+1}) - \ln(R_{i,j}) = \ln\left(\frac{R_{i,j+1}}{R_{i,j}}\right) \tag{6}$$

If we do not use any transformation we simply denote

$$x_{i,j} = R_{i,j}. \tag{7}$$

Lets assume that the spectra is affected by uncontrolled disturbances that have additive and amplificative effects

$$\mathbf{z}_i = \beta_i \mathbf{R}_i^{true} + \alpha_i, \tag{8}$$

where $\mathbf{R}_i^{true}$ are "true" values and α_i represents a offset deviation from some reference level and β_i uncontrolled amplification factor.

If we only measure one single variable, it is impossible to make corrections. But when several variables are measured it is sometimes possible to reduce the effects of these kinds of disturbances. Using the so called multiplicicative signal correction (MSC) method it maybe possible to estimate α_i and β_i and make correction [53]:

$$R_{i,j} \leftarrow (R_{i,j} - \hat{\alpha}_i) / \hat{\beta}_i \tag{9}$$

Orthogonal signal correction (OSC) by Wold et. al (1998) [104] is a new pre-treatment method. In OSC unwanted systematic variation in the spectra is removed by subtracting the components that are as close to orthogonal to the reference values as possible.

4.3 Calculation of calibration parameters

After the pre-treatments and linearizations the problem is to solve unknown parameters **B** of the model:

$$\mathbf{y}_i = \mathbf{x}_i\mathbf{B} + \mathbf{e}. \tag{10}$$

Lets us define matrix **X** with samples $\mathbf{x}_i$ as its rows and matrix **Y** with samples $\mathbf{y}_i$ as its rows. Then the multiple linear least squares (MLR) solution (if it exists) to the problem is

$$\mathbf{B} = (\mathbf{X}^T\mathbf{X})^{-1}\mathbf{X}^T\mathbf{Y}. \tag{11}$$

Because of col-linearity the condition number of $\mathbf{X}^T\mathbf{X}$ can be very big and therefore the estimation error of **B** can be very large (FIGURE 9). So other methods must be used.

4.4 Chemometric tools

Principal component regression (PCR) is one way to deal with the problem of ill-conditioned matrices. The method behind PCR is the principal component analysis (PCA). It finds combinations of variables, (also factors or components) that describe the major trends in data.

Let us consider a *p*-dimensional random variable **x** with covariance matrix *Cov*(**x**). Let $\lambda_1 \geq \lambda_2 \geq \cdots \lambda_p$ be the eigenvalues and $\mathbf{p}_1, \mathbf{p}_2, \ldots \mathbf{p}_p$ be the corresponding eigenvectors of *Cov*(**x**). If **t** denotes the vector of new random

variables, and **P** the orthogonal matrix with $\mathbf{p}_1, \mathbf{p}_2, \ldots \mathbf{p}_p$ as its columns, then **t** is obtained from **x** by the orthogonal transformation

$$\mathbf{t} = \mathbf{xP} \tag{12}$$

The random variable t_i is called the i^{th} principal component of **x**.

The principal components have the following interesting properties. Suppose we want to replace the p-dimensional random variable **x** by smaller k-dimensional random variable without much loss of information. Then the best choice is to use the first k-principal components, if the linear projection functions are to be used [73].

With the principal components we can model the information in **X**

$$\mathbf{X} = \mathbf{T}_k \mathbf{P}_k^T + \mathbf{R} \tag{13}$$

where **R** is matrix of residuals and $\mathbf{T}_k$ is matrix with k-principal components as its columns and $\mathbf{P}_k$ is the matrix of corresponding k-eigenvectors as its columns.

The principal component regression (PCR) consists of the following steps: first select a group of principal components which span the predictor space and then the ordinary least squares is performed on selected vectors. After that the calibration coefficients **B** can be calculated using the eigenvectors.

A very important question is which principal components should be included in the model. There are two partially conflicting objectives. In order to eliminate errors due to multi-col-linearities, it is essential to delete all of those components, whose variances are very small but, at the same time, it is undesirable to delete components which have strong correlation with the dependent variable **Y**. In standard PCR first A- components whose variances are largest are selected.

Standard version of PCR:

Step 1. Calculate principal components

$$\mathbf{T} = \mathbf{XP} \tag{14}$$

Step 2. Perform least squares regression of **Y** on $\mathbf{T}_A$ which is matrix of first A-columns of **T**

Step 3. Calculate the calibration parameters

$$\mathbf{B} = \mathbf{P}_A (\mathbf{T}_A^T \mathbf{T}_A)^{-1} \mathbf{T}_A^T \mathbf{Y} \tag{15}$$

Selection based on variance is an attractive and simple strategy. However, low variance for a component does not necessarily imply that the corresponding component is unimportant in the regression model. In contrast to selection based on size of variance, the opposite extreme is to base selection only in order of correlation of principal components with **Y** or order of t-values.

Partial least squares (PLS) is related both to PCR and MLR and can be though of being between them. PCR finds components that capture the greatest amount of variance. MLR uses every variable and tries to find out their

correlation to reference values at the same time. The intention of PLS is to form components that capture the most of the information in the **X** variables that is useful for predicting **Y**, while reducing the dimensionality of the regression problem.

PLS can be described shortly as follows [25]. Other forms of PLS algorithm can be found in [53]. Let us define $\mathbf{S} = \mathbf{X}^T\mathbf{X}$ and $\mathbf{s} = \mathbf{X}^T\mathbf{Y}$ and weights $\hat{w}_1 = \mathbf{s}$.

Step 1. Calculate the sequence

$$\hat{w}_{A+1} = \mathbf{s} - \mathbf{S}\hat{\mathbf{W}}_A(\hat{\mathbf{W}}_A^T\mathbf{S}\hat{\mathbf{W}}_A)^{-1}\hat{\mathbf{W}}_A^T\mathbf{s}, \quad \hat{\mathbf{W}}_A = [\hat{w}_1, \hat{w}_2, \hat{w}_3, ..., \hat{w}_A]$$

Step 2. Calculate the calibration parameters

$$\mathbf{B} = \hat{\mathbf{W}}_A(\hat{\mathbf{W}}_A^T\mathbf{S}\hat{\mathbf{W}}_A)^{-1}\hat{\mathbf{W}}_A^T\mathbf{s}, \tag{16}$$

Recently Stone and Brooks [90] have unified MLR, PCR and PLS under a single technique, Continuum Regression (CR). By selecting the so called continuum parameter one can choose a method continuously between PLS and PCR or between PLS and MLR

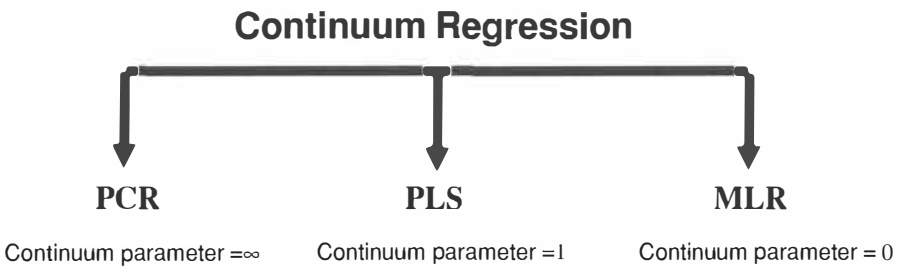

FIGURE 8. *Relationship between PCR, PLS, MLR and CR.*

4.5 Validation

The prediction ability is of course the most important property of an analyzer. In practice the mean square error of prediction (MSEP) can be estimated by simply computing the average squared difference between actual and predicted value, i.e.

$$\text{MSEP} = \frac{1}{K}\sum_{k=N+1}^{N+K}(y_k - \tilde{y}_k)^2 \tag{17}$$

for a set of objects not included in the calibration. The square root of estimated MSEP may be preferable, because this is measured in the same units as y_j itself. It is denoted RMSEP (root mean square error of prediction).

The standard error of prediction (SEP) is defined

$$\mathrm{SEP} = \sqrt{\frac{1}{K}\sum_{k=N+1}^{N+K}(y_k - \tilde{y}_k - \bar{e}_p)^2}$$

where $\bar{e}$ is the bias

$$\bar{e}_p = \frac{1}{K}\sum_{k=N+1}^{N+K}(y_k - \tilde{y}_k)\,. \tag{19}$$

The MSEP, SEP and bias are related to each other:

$$\mathrm{MSEP} = \bar{e}_p^2 + \mathrm{SEP}^2\,. \tag{20}$$

The drawback of the method is that it is rather wasteful to keep aside a large and representative set of test objects only for testing purposes. It would be more economical to use all available data both for calibration and testing.

When the predictor is tested on the calibration set itself we easily obtain the so called standard error of calibration (SEC) defined as

$$\mathrm{SEC} = \sqrt{\frac{1}{N}\sum_{k=1}^{N}(y_k - \tilde{y}_k - \bar{e}_c)^2} \tag{21}$$

where $\bar{e}_c$ is the bias

$$\bar{e}_c = \frac{1}{N}\sum_{k=1}^{N}(y_k - \tilde{y}_k)\,. \tag{22}$$

SEC must be considered more as a lower bound for prediction ability rathe than a measurement of the prediction ability itself. A real measure of prediction ability will have to bring into account the estimation error of the parameters as well. It is usually possible to get a very small calibration error by introducing a more complex model with many independent parameters, but the prediction ability of that model can be very bad (see FIGURE 9).

Cross validation is a better internal validation method. In full cross validation the calibration is repeated N times, each time one of the object is left out from calibration set and treated as prediction object. In the end all the calibration objects have been treated as prediction objects. The estimate of the mean square error, can be computed using the formula (17) for prediction objects. That estimate is called the mean square error of cross-validation (MSECV). Its square root is denoted RMSECV.

4.6 Optimal modelling complexity

Multivariate calibration aims at reducing the prediction error by modelling physical interference phenomena that would otherwise destroy concentration determinations. Each independent interfering phenomena requires an independent factor dimension in the multi-dimensional calibration model. As FIGURE 9 shows a minimal prediction error is attained at a certain number a calibration factors.

The prediction error is composed of two main contributions: the calibration error and the estimation error.

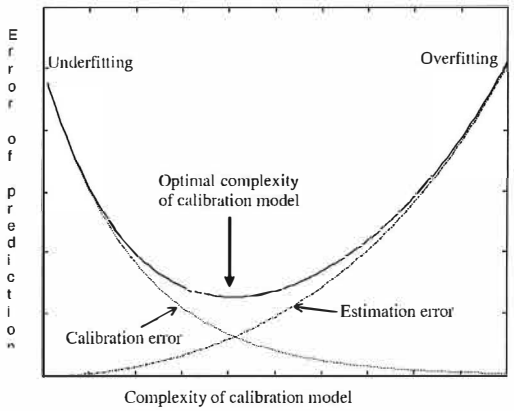

FIGURE 9. Validation [53]: Conceptual illustration of prediction error as a function of complexity of calibration model. Over- vs. underfitting. The arrow indicates optimum.

If the calibration objects are sufficiently representative, the calibration error should decrease with an increasing number of interferences being modelled. At the same time the estimation error of parameters increases due to the increase of the statistical uncertainty when the number of independent model parameters is increasing. That is why only a limited number of independent parameters can be estimated with high precision from a given set of calibration data.

The most used technique to select the number of dimensions in practice is to compute the prediction ability for the different number of factors for the calibration data and then draw up a graph. The estimation for the prediction error can be computed using either prediction testing or cross-validation.

4.7 Detection of the outliers

Detection of abnormal observations (or outliers) is important because they may have great influence on the calibrating results. There are different kinds of

errors: errors in spectral values **X** and errors in laboratory measurements **Y.** Multivariate calibration offers powerful tools for outlier detection.

In the calibration set we know the reference values for the predicted values, and hence we can calculate the corresponding residuals. By scaling the residuals $\mathbf{e}_i$ by dividing them by an estimate of standard error, the improved diagnostics may be obtained. These scaled residuals are called Studentized residuals.

Some outliers will have greater effect on the regression estimates than others. This leads to the use of simultaneous testing procedures.
A sample that has particularly high leverage

$$h_i = \mathbf{t}_i^T \left(\mathbf{T}^T \mathbf{T}\right)^{-1} \mathbf{t}_i , \tag{23}$$

in the calibration set will not necessarily have relatively low residual irrespective of its true error level (Weisberg [102]). That kind of outliers will not allways be detected by looking residuals only.

A low leverage for an object shows that the object is close to the centre of the calibration set and has very little importance for the calibration solution. A calibration object with high leverage may have a strong effect on the resulting calibration model.

Once outliers are detected the problem is only half solved. One must decide either to remove them from the model or keep them. Samples that have low studentized residuals and high leverage are difficult to judge. If there is nothing wrong with their measurements, they contain unique information about the data. If similar samples may be seen in future predictions, they should be kept in the model.

5 CONSISTENCY MEASUREMENT BASED CONTROL SYSTEM

The development of measurements and control systems for the TMP-process started in 1985 as a co-operation project with Rauma-Repola OY, Kymi-Strömberg OY (a part of ABB nowadays) and Tampere University of Technology.

In the beginning of the project a periodical disturbance in the refiner motor loads was detected (FIGURE 10). In that mill the operator usually compensates for this kind of disturbance by changing the set point of the dilution water flows.

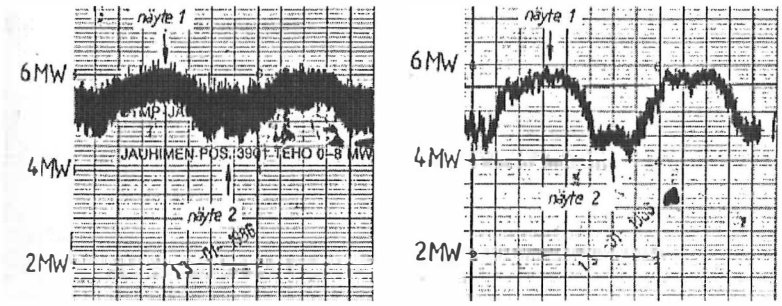

FIGURE 10. The effect of raw material variations on the motor loads of the first and second stage refiner [36].

The reason for the phenomena in FIGURE 10 was that the chips were sorted according to their weight, when they were blowed to the chip pile. The chips were collected by the collection screw which moved under the chip pile from the place where chips were blowed to the other end of the pile. The length of the period of the collection screw was the same as the length of the period of the disturance in FIGURE 10. It remained unclear whether the reason for difference in weight of the chips was the difference in chip moisture or difference in the thickness of the chip or both.

During the mill tests we realized how important it would be to be able to measure the real production rate and chip moisture. We tested the belt weigher to measure chip density and infra-red method to measure chip moisture, but without any succes.

The idea to measure consistency of TMP pulp by near infrared technology was tested of-line at the Tampere University of Technology in 1986 and later patented by Pietinen and Savonjousi [69]. The first results were encouraging and led to intensive research and product development together with Technical Research Center of Finland (VTT).

The prototype of TMP Consistency Analyser (TCA) was installed in the blow-line of the small TMP refiner in Kyröskoski in 1988. In that mill a new method to control the mass flows around the TMP refiner was developed and first published by Saarinen and Savonjousi 1989 [78].

The new idea is based on the assumption that when all other control loops around the refiner are accurate enough, the motor load is a two dimensional function of the inlet consistency and production rate. On the other hand, outlet consistency, inlet consistency, production rate and motor load are connected together by energy and mass balance equations (e.g. equation (7)). When the plate gap is kept constant, the production rate and inlet consistency can be stabilized by stabilising the outlet consistency and motor load. In this way, constant specific energy and refining intensity can be preserved in order to achieve uniform pulp quality.

The basic control for the primary refiner consists of a multivariable adaptive control algorithm with two control loops: consistency and fibreflow (FIGURE 11). The consistency after the refiner is controlled by manipulating the dilution water flow and the fibre flow is controlled by manipulating the speed of the chip feeder based on motor load measurement. The process response is non-linear and dependant on a number of factors (Chapter 3). For good control results the system must react to disturbances rapidly, taking into account the changes in process dynamics and gains as well as cross-coupling between variables. The adaptive consistency control is presented in publications [I] and [III].

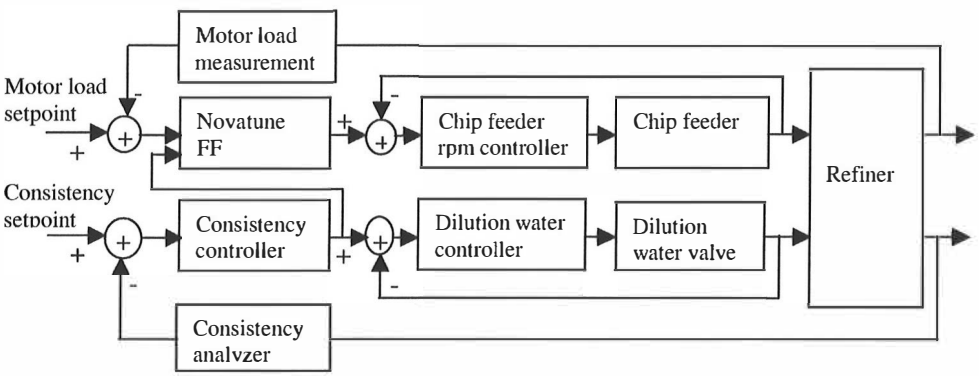

FIGURE 11. AutoTMP /refiner control [III]

In the following the NIR technique based consistency measurement called TCA (TMP Consistency Analyser) and the adaptive model predictive consistency consistency control are shortly described.

5.1 Consistency measurement

The consistency measurement is based on the reflection of near infrared light and takes place directly in the steam and pulp flow from the refiner. The measurement utilizes the resonance vibration of water, which appears as absorption bands in the infrared region of the spectrum.
In the near infra-red (NIR) region of the spectum strong absorption is observed at 1450 nm due to second harmonic of the O-H stretching vibration.The absorbtion at 1930 nm is a combination frequency of O-H bend and the asymmetric O-H strech vibration, and is charasteristic of absorption in water (FIGURE 12).
Four wavelength bands of the spectrum are used by the TCA to evaluate the pulp consistency. The bands are selected such that two of them are located in the absorption bands of water (1.45 μm and 1.93 μm) and the other two in a region where the effect of water is small (1.70 μm and 2.10 μm).

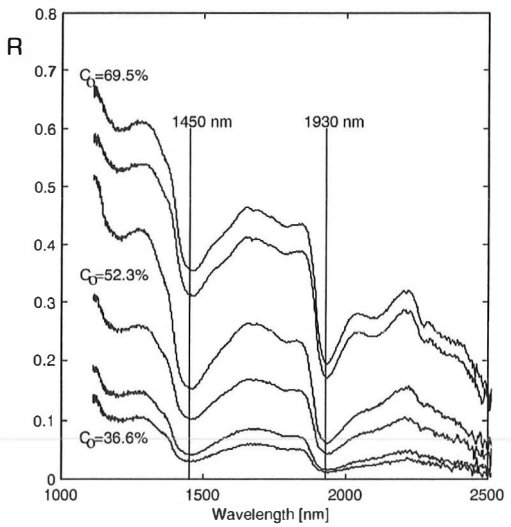

FIGURE 12. Near infra-red reflectance spectra of TMP pulp samples with different consistencies. Measured in the laboratory of VTT, Oulu.

TCA sensor consist of a probe connected by optic bundles to a measuring unit with a infrared light source and a multi-wavelength detector which can simultaneouly record four different wavelengths. The probe is mounted in the process line together with an interface unit and can be removed and refitted

during operation. The measuring unit transmits from the process to a computing unit.

The calibration method for TCA was developed by Saarinen [80, 82]. We tested first different types of single band and two-band models with MLR method. We experienced in practice the following problems, which are common in the calibration of an NIR analyser [53]:

- *Lack of selectivity*: No single wavelength band was sufficient to predict the wanted value.
- *Col linearity*: There was strong correlation between different wavelength bands.
- *Lack of knowledge*: Our prior understanding of the mechanism behind the data was incomplete.

Then we tested pre-treatment functions (4)-(7) of Ch. 4 with PCR method and cross-validation technique. The best calibration model that worked in all tested cases was

$$C_O = b_0 + \sum_{k=1}^{3} b_k \left[\ln(R_k) - \ln(R_{k+1})\right]. \tag{1}$$

That model has been used since. FIGURE 13 sumarises the tests results made in 1990 – 1993 in six TMP mills in Europe. The accuracy of the laboratory measurement was estimated in the following way. The pulp samples taken from the blow line were divided into three parts, whose consistency was measured in the laboratory either by owen drying or infra-red drying method. Standard deviation for each pulp sample was calculated. The average value of the standard deviations was used as an estimation of the accuracy of the laboratory mesurements. FIGURE 13 also shows that the accuracy of the TCA is limited by the accuracy of reference method.

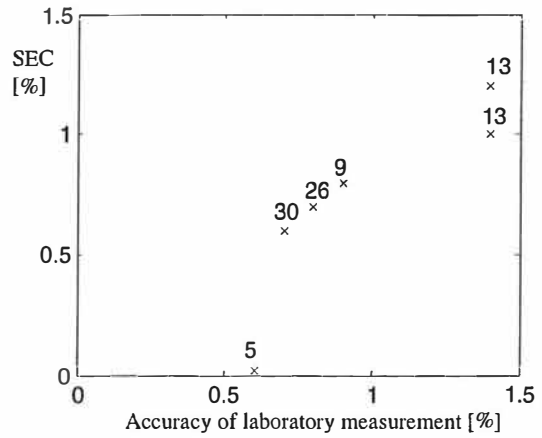

FIGURE 13. Standard error of calibration (SEC) of TCA vs. accuracy of laboratory measurement in six mills (Saarinen [82]). Number of calibration samples is marked above each case.

Field test results during the years 1988 – 1992 has been also reported in [V]. Pietinen and Tiikkaja [70] studied the accuracy of on-line analysers at United Paper Mills Kajaani's TMP plants. They found the standard error of prediction (SEP) for TCA after eight months from calibration to be 0.95 % although some of the test points were outside of the calibration range.

5.2 Adaptive consistency control

The control of the industrial process is complicated in the presence of time delay (often referred as dead time), non-linearities and, if the process behavior changes with time. TMP process has all these properties.

Dead time in consistency control i.e. the time that it takes for a consistency measurement to react when the dilution water flow setpoint is changed, is typically from five to ten seconds. The length of the dead time depends on the location of the place in the process where the dilution water is fed, the location of the TCA and the quality of the dilution water flow control and control valve.

Changes in refining power also change the consistency and thus the dynamic of the dilution flow – the consistency process also depends on the gap and the casing pressure control loops. The response of these loops depends also on the operation point.

In order to run the process close to its limits, the control system must react quickly enough. Due to the non-stationary and non-linear properties of the TMP process mentioned above, the most common controller type in industry, the PID –controller (Proportional-Integral-Derivative), will be either de-tuned or needs to be tuned frequently.

Consideration of the time delay problem led to a development of model predictive control (MPC) strategies independently in France as "model predictive heuristic control" [76] and in the United States as "dynamic matrix control" [12]. Such algorithms have been used succesfully where conventional control algorithms have failed [76],[71]. The major advantage of MPC is that the control algorithm can be made robust, or insensitive to modelling errors, in a direct way [76]. MPC is a class of control algorithms that utilize process models for predicting future process outputs and computing corrective actions to achieve the desired target values. Control actions are calculated by minimising the least-squares objective function based on the residuals between the model predictions and the desired set point profile over the prediction horizon. Only the first control move is actually implemeted and the next process measurement is obtained. The model is updated and a new optimization problem is solved at next time step. When linear models and quadratic objective functions are used, the optimization problem reduced in a quadratic programming. The adaptive consistency contol is presented in the publications [I] and [III]. The very important part of the MPC is a reliable process model, which is identified on-line in order to give as accurate

predictions as possible. Selected process model together with identification algorithm is presented briefly in the following. A more detailed description of the on-line identification algorithm is presented by Saarinen in the appendix of [82].

5.2.1 Process-model

Models based on physics of the refining process are either static or too complex to be used for control purposes. If we assume that a linear model can be used near an operation point, we can start model selection from a general family of linear discrete black-box single input – single output model structures [50]

$$A(q^{-1})y(t) = \frac{B(q^{-1})}{F(q^{-1})}u(t) + \frac{C(q^{-1})}{D(q^{-1})}\xi(t), \tag{2}$$

where q^{-1} is delay operator

$$q^{-1}f(t) = f(t-1), \tag{3}$$

u is input, y is output, and ξ is white noise. Examples of the polynomials are presented in more detailed in formula (6).

The general model is too complex for most practical purposes. By fixing one or several of the five polynomials to unity, we get models that are easier to use. Some of the common special cases are presented in the table below.

TABLE 2. Some common Black-Box single input – single output models as special cases of (2) [50]

Polynomials used in (2)	Name of the model structure	Abrev.
B	Finite Impulse Responce (FIR)	FIR
AB	Auto Regressive with eXtra input	ARX
AC	Auto Regressive Moving Average	ARMA
ABC	Auto Regressive Moving Average with eXtra input	ARMAX
ABD		ARARX
ABDC		ARARMAX
BF	Output error	OE
BFCD	Box-Jenkins	BJ

Yeat another version with enforced integration in the system description is obtained by replacing $y(t)$ in ARMAX model by $\Delta y(t)=y(t)-y(t-1)$. The model is called ARIMAX.

The Wold composition theorem [103],[40] states that any wide sens stationary process can be decomposed into a component that is completely random and the one that is deterministic. A corollary of Wold's theorem states that any AR or ARMA process can be represented by a unique MA process of infinite order [40]. A theorem due to Kolmogorov [44] states that, similarly, any ARMA or MA process can be represented by an AR process of finite order.

These theorems are important because if we choose wrong model among the three, a reasonable approximation may still be obtained.

One of the pre-requisites for advanced controllers is that they should be easy to commission. We selected an incremental type of model, because it is easy to understand and initial values for parameters can be obtained by simple step response test

$$\Delta c_O(t) = H(q^{-1})\Delta u(t)q^{-d-1} + \frac{C(q^{-1})}{D(q^{-1})}\Delta\xi(t), \tag{4}$$

where d is the dead time of the process, Δ difference operator

$$\Delta f(t)=f(t)-f(t-1) \tag{5}$$

and

$$\begin{aligned} H(q^{-1}) &= h_1 + h_2 q^{-1} + ... + h_{N_h} q^{-N_h-1} \\ C(q^{-1}) &= 1 + c_1 q^{-1} + ... + c_{N_c} q^{-N_c} \\ D(q^{-1}) &= 1 + d_1 q^{-1} + ... + d_{N_d} q^{-N_d} \end{aligned} \tag{6}$$

c_O is measured consistency after the refiner, u is set point to the dilution water flow controller and ξ is white noise.

5.2.2 On-line identification

The identification process model in closed looped control systems requires certain conditions in order to work properly. It has been shown in survey paper by Gustaffson et. al. [22] that identification is possible in a variety of feedback situations; when an extra input signal is applied, when the set point to the regulator is varied, when there is noise in regulator, or when the regulatror is time-varying or non-linear. In these cases the system is strongly identifiable. Our controller is time-varying, since the parameters are continuously updated. The recursive Gauss-Newnton on-line identification algorithm used in our consistency controller is described below.

The problem is to minimize the cost function J with respect to unknown parameters θ

$$\min_{\theta} J(t,\theta) = \sum_{i=1} \gamma^{t-i}\varepsilon(i,\theta)^2 \quad ; t = 1,2,3,...$$

where γ is so called forgetting factor, ε one step prediction error

$$\varepsilon(i,\theta) = \Delta c_O(i) - \theta(i)^T \Phi(i,\theta)$$

and

$$\theta^T(i) = [h_1, h_2, ..., h_{N_h}, d_1, d_2, ..., d_{N_d}, c_1, c_2, ..., c_{N_c}]$$

$$\Phi^T(i) = [\Delta u(i-d-1), \Delta u(i-d-2), ..., \Delta u(i-d-N_h), \Delta v(i-1), \Delta v(i-2), ..., \Delta v(i-N_d), \Delta \xi(i-1), \Delta \xi(i-2), ..., \Delta \xi(i-N_c)]$$

are the parameter vector and the "state vector" respectively.

Recursive identification algorithm using stochastic Gauss-Newton searching direction can be summarized as follows:

1. Select forgetting factor γ, initial values for matrix $\mathbf{P}(0)$ and parameters $\theta(0)$. Set t=1 and gradient $\psi(0) = \Phi(0,\theta)$.
2. Update state vector Φ
3. Calculate and limit the prediction error

$$\varepsilon(t,\theta) = \Delta c_O(t) - \theta(t)^T \Phi(t,\theta)$$

$$\varepsilon_\ell(t,\theta) = \begin{cases} -\alpha_\ell & ; \varepsilon(t,\theta) < -\alpha_\ell \\ \varepsilon(t,\theta) & ; |\varepsilon(t,\theta)| \le \alpha_\ell \\ \alpha_\ell & ; \varepsilon(t,\theta) > \alpha_\ell \end{cases}$$

4. Calculate

$$\mathbf{L}(t) = \frac{\mathbf{P}(t-1)\psi(t-1)}{\psi^T(t-1)\mathbf{P}(t-1)\psi(t-1) + \gamma}$$

5. Update the parameters

$$\theta(t) = \theta(t-1) + \mathbf{L}(t)\varepsilon_\ell(t,\theta)$$

6. Update $\mathbf{P}$

$$\mathbf{P}(t) = \frac{1}{\gamma}[\mathbf{I} - \mathbf{L}(t)\psi^T(t-1)]\mathbf{P}(t-1)$$

7. Update the gradient ψ

$$\psi^T(t) = [\Delta\tilde{u}(t),...,\Delta\tilde{u}(t-N_h+1),-\Delta\tilde{v}(t),...,-\Delta\tilde{v}(t-N_d-1),$$
$$\Delta\tilde{\xi}(t-N_c-1),...,\Delta\tilde{\xi}(t-N_c-1)]$$

$$\Delta\tilde{u}(t) = \Delta u(t-d-1) + d_1\Delta u(t-d-2) + ... + d_{N_d}\Delta u(t-d-N_d)$$
$$- c_1\Delta\tilde{u}(t-1) - ... - c_{N_c}\Delta\tilde{u}(t-N_c)$$
$$\Delta\tilde{v}(t) = \Delta v(t) - c_1\Delta\tilde{v}(t-1) - ... - c_{N_c}\Delta\tilde{v}(t-N_c)$$
$$\Delta\tilde{\xi}(t) = \Delta\xi(t) - c_1\Delta\tilde{v}(t-1) - ... - c_{N_c}\Delta\tilde{v}(t-N_c)$$

8. $t \leftarrow t+1$, go to 2.

5.3 Quality control

The consistency and fibre flow control provide the basis for the efficient quality control and optimization of the refiner line. When the refining process proceeds steadily and effective compensation is provided for the disturbances, the quality of the pulp is easier to sustain.

During the summer of 1991 a series of process tests were undertaken to determine the effect of consistency, power split, and specific energy on the pulp quality (freeness, tear index, tear index and fibre length) by Saarinen [79]. So called central composite design of experiments [64] was used in order to get reliable models with a minimum number of test points. Part of the results are also presented in [IV] and [V].

FIGURE 14 shows the effect of consistency on tear and tensile index, when the specific energy, and the production rate are kept constant. Each of the three curves represents different power splits (percentage of the total specific energy used by the first stage refiner) and each point in the curve represents different outlet consistency - plate gap combination of first stage refiner. The consistencies at the points of the maximum tear index in each curve are all 42 % and they correspond to the maximum plate gaps, that can be used to maintain the required specific energy. (See also FIGURE 3, FIGURE 8 in [II] and FIGURE 1 in [IV])

The reason for this is that the average fibre length is mainly defined by the operation of the first stage refiner and tear index is strongly related to the average fibre length. The longer the fibres are the bigger the tear index is. On the other hand the average fibre length is mainly defined by the plate gap.

The quality of TMP pulp can be described by three variables (Chapter 3.2): freeness, fibre length distribution and shives content. By controlling these variables the paper making properties of the refiner pulps (i.e. their strength and optical properties) are maintained at their optimal values or at least whithin the allowable range.

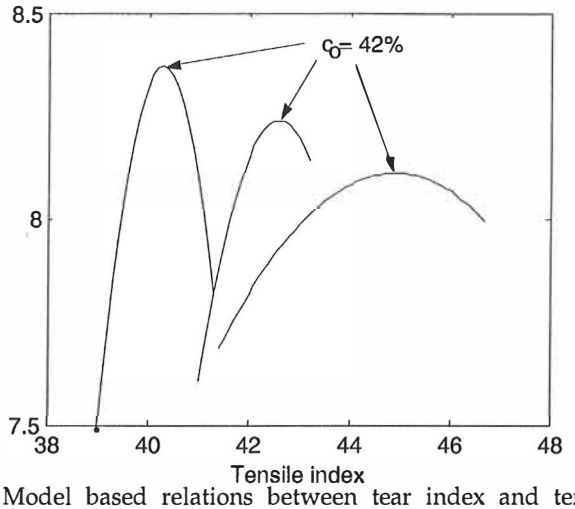

FIGURE 14. Model based relations between tear index and tensile index with three different power splits, when specific energy and production rate are kept constant [79].

In the case of the two-stage refining process, there are two quality variables that have to be controlled by four control variables: the consistencies, the specific energy and the power split. Here we have assumed that shives are controlled by changing the pulp flow to the reject refiner and the production rate is not included in the control strategy.

The selection of the final quality control strategy is based on mill evaluations according to experience and/or mill tests. In AutoTMP [VI] the quality control is based on model reference control where set points for control variables are calculated on the basis of analyzer readings, quality models, previous control actions and the dynamic model for the latency chest.

In Papeterie du Golbey application [VI] the freeness control was carried out by changing specific energy consumption. If only freeness is controlled, the power split remains unchanged, unless the power intake in one of the refining stages meets its upper/lower limits. In AutoTMP control the consistency set point of the first stage refiner is kept at its optimal value (see FIGURE 14) and specific energy is controlled by manipulating the plate gaps. This procedure quarantees that the optimum consistency is continuously maintained and the changes in freeness are fastly corrected.

The fibre length distribution is controlled by changing the power split between the stages; i.e. by searching for the compination of consistency and gap that maintains the required freeness with maximum fibre length.

In Papeterie du Golbey France the system has been in productive usage since 1991 and very soon gained operator acceptance.

5.4 Results of field tests

The first step in any control design should be the study of the disturbances. Although the effect of the disturbances can be seen in refining power, at least a second measurement is needed in order to distinguished between a chip moisture and production rate disturbance. With the blow line consistency measurement it was possible to estimate the feed disturbances based on mass and energy balance calculations around the refiner. These disturbances and their effects are reported in [II].

We found up to 10% variations in chip moisture content and up to 15 % relative variations in production rate. It is easy to understand that conventional balance based control strategies or single loop control strategies have had serious difficulties in these kind of circumstances.

The first AutoTMP/Refiner control system was installed in a Finnish mill in 1988. The results were very encouraging. For example the benefits of the adaptive control system was clearly proved , variations in consistency and refiner motor were reduced significantly and the production rate could be increased by 10 %. Since then over 90 systems have been installed. The test results during the years 1988 – 1992 in Nordic mills are summarised in [V].

The purpose of the basic refiner controls is to maintain the refiner stability in such a way that the uniform pulp quality is achieved. Results in TABLE 3 show that AutoTMP/Refiner control system has reached this target.

TABLE 3. Comparison of convential control system and AutoTMP/Refiner control system in two TMP mills. Std means standard deviation and diff is the difference of the standard deviations in percentage diff = 100%*std(On)/std(Off)-100%.

	Tasmanian Pulp & Paper Co. Ltd 29.1-2.2.1999						UPM Kajaani 1992
	Line #1			Line #2			
AutoTMP control mode	Off	On	diff	Off	On	diff	diff
	std	std		std	std		
Consistency, Primary[%]	2.02	1.03	-49	2.27	1.26	-44	-76
Consistency, Secondary [%]	4.31	1.19	-72	4.45	1.71	-61	
Motor load, Primary [MW]	0.32	0.20	-39	0.34	0.24	-28	-70
Motor load, Secondary [MW]	0.60	0.27	-56	1.16	0.61	-48	-70
Freeness [ml]	23.3	11.3	-52	31.8	10.8	-66	-76
Tensile index [Nm/g]	1.9	1.3	-31	3.5	2.1	-40	-89
Tear index [m Nm2/g]	0.84	0.76	-10	1.10	1.00	-9	-82

6 CHARACTERIZATION OF TMP PULP BY NEAR INFRA-RED MEASUREMENT

TCA was thoroughly tested at two mills in Norway in 1990-1991. Due to the fact that the simple calibration model did not work properly, also freeness and tear index values of the calibration samples were measured in order to find out the factors that affect the consistency measurement. This led to the development of the PCR calibration method for consistency measurement but as a side effect a good correlation between freeness and TCA signals was found. The new method to measure TMP freeness was patented by Saarinen for the first time in Finland [81] and then in the USA [VII]. With non-linear pre-treatment of the TCA signals and the PCR calibration method, the standard error of calibration (SEC) in freeness calibrations where 13 ml and 24 ml VII. As a result of this a product development project was started and a new analyser called TQA (TMP Quality Analyzer) was developed in ABB.

TQA measures 24 wavelength bands from the NIR spectrum by SpectraFlas array detector system. It is mounted in the same way into the process as TCA, and thus provides a truly continuous in-line measurement of the process.

TQA has been tested in TMP mills in Finland. Currently we can measure freenes, tensile index and Bauer-McNett fibre length distribution with TQA. The problem is that at the moment the best method in looking for calibration model is trial and error method. The drawbacks of this kinds of "black-box" approach are:

- many calibration samples are needed
- it is not known what physical properties are really measured
- there is uncertainty about the factors that has effects on the measurement
- calibration is not general: new calibration is needed in every installation.

It is obvious that understanding the scattering charasteristic of various paper particles in different measurement situations plays an important role when we want to develop new analysers and reduce calibration work. For this reason we

have started a research project at ABB Corporate Reseach OY considering light scattering by paper particles. The objectives of the project are:

- to have a better understanding of the scattering phenoma
- to be able to find the optimum
  - combination of scattering matrix elements to be used for
  - measurement
  - selection of wavelength bands
  - measurement geometry
  - calibration model and method.

The vision is to have "plug and measure" -analysers in future.
In addition to theoretical studies we have made light scattering measurements in different laboratories in Germany, Italy and Finland. Part of the studies have been published in [VIII] and [IX].

In what follows we present the most interesting examples of calibration of TQA with multivariate methods. After that we study layered circular cylinder theoretically. Then we shall shortly introduce the new stochastic wood fibre model based on papers [VIII] and [IX] together with geometric optics method. To validate the geometric optics approach, we compare the geometric optics and exact results for layered circular cylinder. We will also give new simulation results which show the effects of shape parameters on the single-particle albedo and asymmetry parameter, which are the two most important light scattering charasteristics of a single wood fibre.

6.1 Statistical models

Test results from two mills are presented in the following. In both mills TQA was installed after second stage refiner, with a push-button near the sampling place for spectra regording. At the same time when a pulp sample was taken, the button was pushed and TQA saved the corresponding spectra with time stamps in its memory. Later the spectra were exported to personal computer.

During the test periods the operation parameters were changed as much as possible in such a way that the correlation between consistency and freeness would be as small as possible. It should be noted that all the tests were made during normal production circumtances, so it was not possible to produce very bad quality pulp or risk the continuos operation. In statistical calculations MATLAB software with Data analysis toolbox [23]. was used. Outlier detection and data pre-treatment methods were programmend by author.

6.1.1 Tests in mill I

In the mill, which here is called mill I, nine tests runs were made during one year. The samples were grouped into three sets (TABLE 4). Samples were

analysed at University of Oulu, Finland. From all samples the consistency and freeness was measured. From samples belonging to the calibration and test set 1 also handsheet was made from which tear and tensile index was measured.
Inspite of the changes made in operation variables, the standard deviation of tear index was only 0.38 mNm^2/kg, which was only about 4% of its mean value 8.11 mNm^2/kg. For this reason we did not try to make a tear index model.

It is important to calculate the correlations between the laboratory values, because if there is a strong correlation between modelled values and some other value it is impossible to say which of these values the analyser is realy measuring. The correlation matrix of laboratory values is in TABLE 5. We can see that there is rather weak correlation between the values.

TABLE 4. Data groups in mill I.

Date	Name of the group	Number of samples (Outliers removed)
24. 5.2000 – 4. 7.2000	Calibration set	25
24.10.2000 – 22.12.2000	Test set 1	25
14.02.2001 – 6. 3.2001	Test set 2	23

TABLE 5. Correlation matrix of laboratory values at mill I: Co=Consistency, CSF=Freeness, and Ten=tensile index, respectively.

	Co	CSF	Ten
Co	1.00	-0.34	0.04
CSF	-0.34	1.00	0.26
Ten	0.04	0.26	1.00

Freeness models

We have tested a large number of different kinds of transformation equations, wavelength band combinations and pre-treatment methods like MSC and OSC in order to find out a good model for freeness calibration. It is not our intension to present all of the test results, but illustrate the effects of different pre-treatments together with the best model found so far. The notations for the models used in this chapter are following (see also Chapter 4.2):

Notation	Model	
iden	$x_i = R_i$	
ln	$x_i = \ln(R_i)$	(1)
ln(i)-ln(i+1)	$x_i = \ln(R_i) - \ln(R_{i+1})$	
K-S	$x_i = \frac{1-R_i^2}{2R_i}$,	

where R_i is reflectance at band i,(i=1,...,24) measured by TQA. The original Kubelka-Munk transformation is

$$x_i = \frac{(1-R_i)^2}{2R_i} \tag{2}$$

FIGURE 15 shows the effect of the proposed K-S transformation. It inverts the spectra and amplify the bands in which water has absorption peaks. Especially band 18 is amplified greatly. Because band 18 has very strong correlation to water content of the pulp, we have tested models in which we have excluded that band, when we modelling quality values.

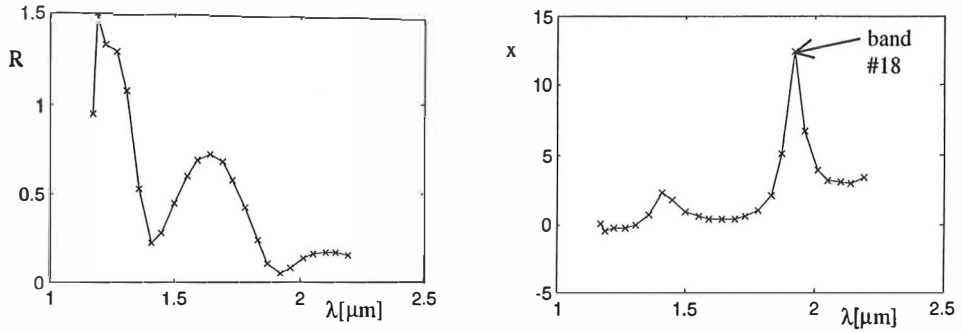

FIGURE 15. The effect of K-S transformation on TQA spectra. Average of measured spectra is on the left. Average of K-S transformed spectra is on the right. Wavelength at the centrum of each band is marked with 'x'.

TABLE 6 summarises the results for freeness calibrations. We have selected the complexity of the model i.e the number of PLS factors included, using cross-validation (see example in FIGURE 20). However, based on cross validation values (RMSEC) it is difficult to make a decision about which of the models is the better one. The model 8 has the lowest RMSECV value 8 ml and the RMSECV values for the models 4-7 were about the same, 11-12 ml.

The real test for the models is to use an independent test set for validation. The prediction errors (SEP) for test set 1, indicate that the models have very different prediction ability. The model 8 is not the best one any more, K-S type of tranformation gives the best results and MSC pre-treatment does not improve the prediction abilities. Based on the results for test set 1, we can presume that the models 3, 6 and 7 are usable. Further, the prediction errors for test set 1 confirm the assumption that the model that has been calculated using the lowest number of PLS factors has usually the best prediction ability for the future values.

Between test set 1 and test set 2 the mill has decided to increase the value of the consistency setpoint (FIGURE 17). This gave us the possibility to study the extrapolation ability of the models. Results for test set 2 in TABLE 6 show

that only model 7 has an acceptable standard error of prediction, but the bias 48 ml is too large. The prediction ability of the models 3 and 7 is futher illustrated in FIGURE 16.

FIGURE 18 shows the comparison of freeness measured in laboratory and calculated by TQA using the models 3 and 7, when all samples except outliers form the calibration set. Based on the results in the FIGURE 18 and in TABLE 6 we conclude that model seven is the best one.

Ämmälä et al. have studied the accuracy of laboratory freeness test [106] (TABLE 7). It depends greatly on the analytical skill and routine of the laboratory technician. The most critical step in the whole procedure, however, is usually the sampling of the pulp from the process. Mean value of our CSF values measured at laboratory was 164 ml. This means that the best SEP that is possible to reach is in relative units 4 % , which corresponds 7 ml in freeness units.

The SEP and RMSECV values 11 ml for model 7 in TABLE 6 and in FIGURE 18 b), respectively, are rather good results when taking into account the facts that; there is, inspite of the control system, some specific energy variations left in the process, pulp is flowing with high speed in the blow-line, and the sample that is taken from the proces is never measured by TQA since the sample taking place is much nearer to the refiner than TQA.

TABLE 6. Performance of different calibration models in predicting Canadian Standard Freeness. Notations for models are explained by (1). Number 18 in parnthesis (18) means that the band is excluded from the model. MSC means multiplicicative signal correction (see Chapter 4.2)

Model	Pre-treatment	PLS factors	Calibration set		Test set 1		Test set 2	
			SEC [ml]	RMSECV [ml]	SEP [ml]	Bias [ml]	SEP [ml]	Bias [ml]
1	Iden	4	11	14	23	-11	64	-27
2	Iden + MSC	4	11	14	18	-4	21	16
3	ln	5	9	12	17	-9	42	-41
4	ln + MSC	6	8	11	23	1	51	5
5	ln(i+1)-ln(i)	6	8	11	26	1	26	-45
6	K-S	4	10	11	12	-6	20	-40
7	K-S (18)	4	9	11	11	-4	15	-48
8	K-S (18) +MSC	6	7	8	21	1	63	-12

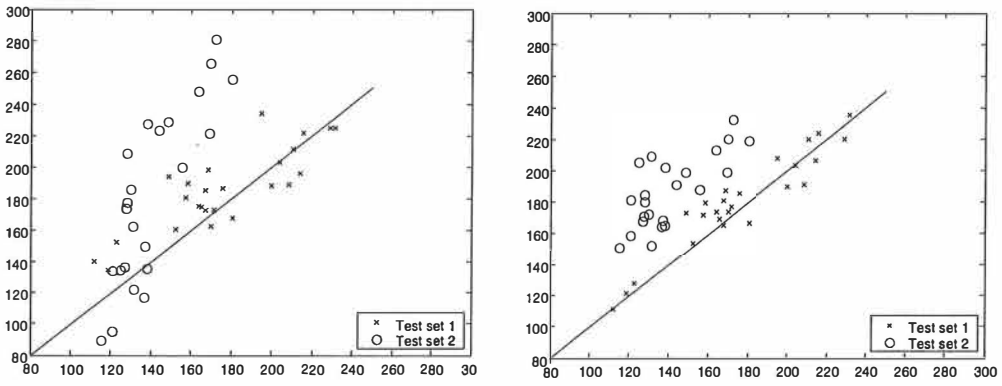

a) b)

FIGURE 16. Prediction ability of the calibration models a) 3 and b) 7 (See TABLE 6)

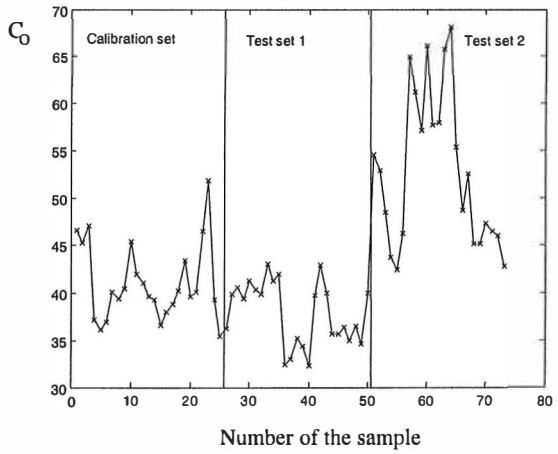

FIGURE 17. Consistency of the pulp samples in test points.

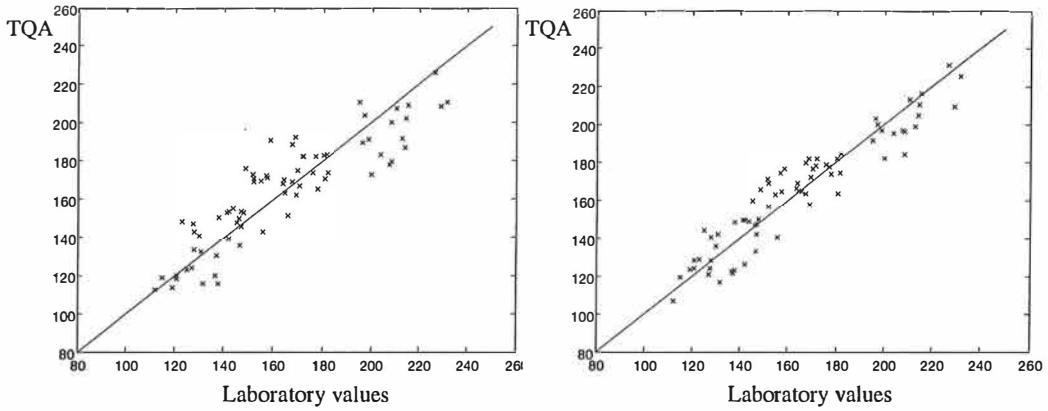

a) b)

FIGURE 18. Comparison of CSF [ml] measured in laboratory and calculated by TQA. All samples except outliers form the calibration set. a) model 3 with 6 PLS factors, SEC = 15 ml and RMSECV = 16 ml, b) model 7 with 4 PLS factors, SEC=10 ml, RMSECV=11 ml.

TABLE 7. Accuracy of CSF test in relative units [%] according to Ämmälä et al. [106]

Level of analytical skill	CSF 85 ml Good	Normal	Poor	CSF 130 ml Good	Normal	Poor	CSF 260 ml Good	Normal	Poor
Relative STD [%]									
- Process sampling	5.0	10.0	15.0	4.0	8.0	12.0	3.0	6.0	9.0
- Total	5.3	10.7	16.0	4.4	8.9	13.3	3.5	7.0	10.5

Tensile index models

We have tested a large number of transformation equations, wavelength band combinations together with MSC or without MSC in order to find a good model for tensile calibration. There was an unknown difference between the calibration set and test set 1 that made the prediction ability of the model based only on the calibration set unsatisfactory. For this reason a new calibration set was formed using all available dat for calibration.

FIGURE 19 shows the cross-validation data for the four best tensile index models and FIGURE 20 shows the comparison between tensile index measured at the laboratory and tensile index predicted by TQA with best model according to FIGURE 19 (K-S type of transformation , band 18 excluded ,with multiplicicative signal correction). The relationship between measured and predicted values in FIGURE 19 seems to be non-linear. We conclude that there are connections between the TQA spectra and tensile index, but we have not yet found the best calibration model.

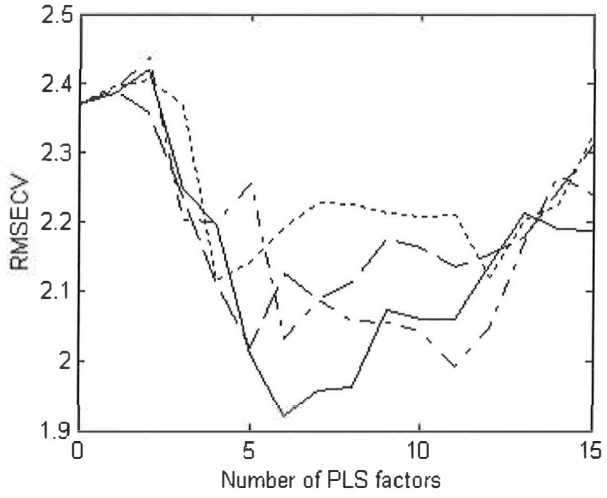

FIGURE 19. Selection of the tensile index model and its optimum complexity. RMSECV [kNm/kg] as a function of number of PLS factors for models K-S (18)+ MSC- (solid), K-S(18) , (dash-dotted), ln (dotted), and ln+MSC (dashed). Notations for models are explained by (1). Number 18 in parenthesis (18) means that the band is exculeded from the model. MSC means multiplicicative signal correction (see Chapter 4.2)

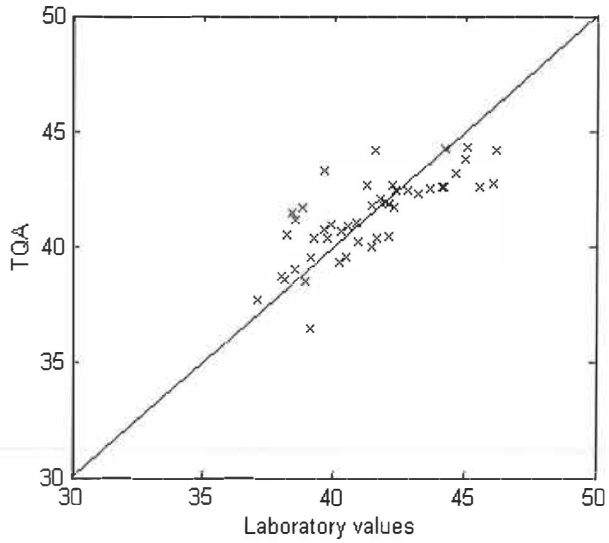

FIGURE 20. Comparison of tensile indexis [kNm/kg] measured at laboratory and calculated by TQA. Samples from calibration set and test set 1 (TABLE 4) whithout outliers form the calibration set. K-S (18) + MSC model with 6 PLS factors was used. RMSECV = 1.9 kNm/kg.

6.1.2 Tests in mill II

In mill II we had a unique opportunity to test the calibration model in extreme conditions, because during the test period they had a plate segment experiment in the mill. We made two test runs, one before the change of the plate segments and another afterwards. From all samples the consistency, freeness and Bauer-McNett fibre classification were analysed at the laboratory of the mill

FIGURE 21 shows the average values and standard deviations of Bauer-McNett classes for plate model A and plate mode B (1=16 mesh, 2=30 mesh, 3=50 mesh, 5=100 mesh,5=200 mesh and 7 <200 mesh (mesh = wires/inch, 200 mesh has 76 µm diameter holes)). The change in average values between the sets is very large for all Bauer-McNett classes, compared to the standard deviations within sets. That large change can not be caused under normal operation conditions with the same plate model. Note that the average freeness and consistency are the same for both data sets (TABLE 8).

Due to the correlations between the different Bauer-McNett classes, 96 % of variations in Bauer-McNett data could be modelled by two principal components, which are denoted by B1 and B2, in the following.

TABLE 8. Data groups in mill II.

Date	Name of the croup	Number of samples (outliers removed)	Plate model	mean(Co) [%]	mean(CSF) [ml]
31.1.2000	Test set 1	28	A	39.6	75
29.2.2000	Test set 2	13	B	40.2	75

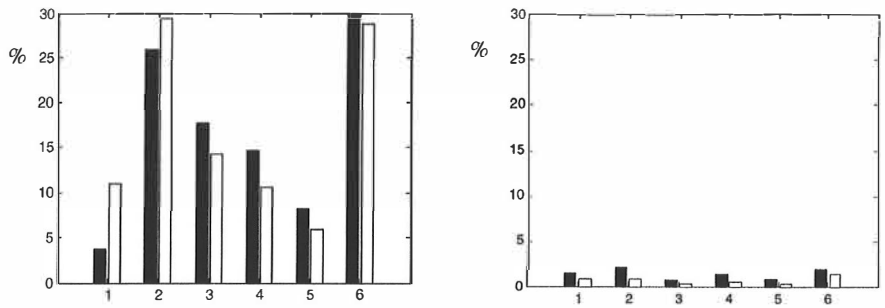

FIGURE 21. Mean values a) and standard deviations b) of Bauer-McNett classification for plate model A (black bars) and B (white bars)

Correlation matrix in TABLE 9 shows that the experiments has succeeded quite well. There is practically no correlation between consistency and freeness. There is some correlation between the second principal component and freeness, which is something to be expected, because both fibre size distribution and freeness are correlated with specific energy.

TABLE 9. Correlation matrix of laboratory values at mill II: Co=Consistency, CSF=Freeness, B1 and B2 are the 1st ans 2nd principal components of Bauer-MCNett classification data, respectively.

	Co	CSF	B1	B2
Co	1.00	-0.08	0.11	-0.07
CSF	-0.08	1.00	0.29	-0.43
B1	0.11	0.29	1.00	-0.00
B2	-0.07	-0.43	-0.00	1.00

Consistency model

Due to the unique change in fibre size distribution we have also tested different consistency models. Test set 1 was used as a calibration set and test set 2 as an independent test set. Results in TABLE 10 show that logarithmic difference model (model 5), that is used in TCA also works best in these extreme conditions.

Freeness model

When modelling freeness, we have found it impossible to predict the freeness values of test set 2 using test set 1 as the calibration set, due to the large change in fibre size distribution. With all values in the calibration set, we achieved the results presented in TABLE 11. Once again the model 7 (K-S transformation band 18 excluded) is the better one

Fibre size distribution model

We tested the same models that we used in testing freenes calibration to model the 1st and 2nd principal components of the Bauer-MCNett classification data (TABLE 11). It is interesting to notice that the best model for the first principal component (model 3) is different than the best model for the second pricipal component (model 7). Accuracy of the models is about the same as the accuracy of the Bauer-McNett method, but quite many PLS factors are needed, which means that the best tranformation equation is yet to be found.

TABLE 10. Performance of different calibration models in predicting consistency. Notations for models are explained by (1). Number 18 in parenthesis (18) means that the band is excluded from the model. MSC means multiplicicative signal correction (see Chapter 4.2)

Model	Pre-treatment	PLS factors	Calibration set Set 1		Test set Set 2	
			SEC [%]	RMSECV [%]	SEP [%]	Bias [%]
3	ln	5	1.0	1.3	1.3	0.2
4	ln + MSC	4	0.9	1.0	1.6	0.3
5	ln(i+1)-ln(i)	2	1.3	1.4	1.3	0.2
6	K-S	4	1.2	1.6	1.4	-1.0
7	K-S (18)	3	1.4	1.6	1.3	-0.7
8	K-S (18) +MSC	5	1.0	1.5	1.9	-0.9

TABLE 11. Performance of different calibration models in predicting the Canadian Standard Freeness. Number 18 in parenthesis (18) means that the band is excluded from the model. MSC means multiplicicative signal correction (see Chapter 4.2)

Model	Pre-treatment	PLS factors	SEC [ml]	RMSECV [ml]
3	ln	5	8	9
4	ln + MSC	4	9	10
5	ln(i+1)-ln(i)	4	8	10
6	K-S	6	7	8
7	K-S (18)	5	7	8
8	K-S (18) +MSC	7	9	12

TABLE 12. Performance of different calibration models in predicting principal components B1 and B2 of Bauer-MCNett classification data. Number 18 in parenthesis (18) means that the band is excluded from the model. MSC means multiplicicative signal correction (see Chapter 4.2). N is the number of PLS factors

	Model	B1			B2		
		N	SEC	RMSECV	N	SEC	RMSECV
3	ln	6	1.5	2.0	5	1.0	1.4
4	ln+MSC	5	1.9	2.4	4	1.1	1.3
5	ln-ln	6	1.8	3.0	5	1.0	1.4
6	K-S	7	1.7	2.4	5	0.9	1.0
7	K-S(18)	7	1.7	2.2	4	0.9	1.0
8	K-S(18)+MSC	7	1.7	2.8	4	0.9	1.3

6.2 Considerations based on physical theories

Near infra-red radiation consists of time-varying electromagnetic fields. The method for computing electromagnetic fields are based on solving Maxwell's equations either analytically or numerically. If want to solve, the problem of light scattering by pulp using Maxwell's equations, we easily find it impossible,

because a smal volume of pulp consists of millions of particles and at least as many boundaries, which boundary conditions we have take care of when solving the equations.

The assumption of independent scattering greatly simplifies the problem of computing multiple light scattering by pulp because it allows us to solve first the single scattering problem and then to use the radiative transfer equation to solve the multiple scattering problem. This is possible, when the distance between the particles is sufficiently large (about 3 times the radius [30]), the particles are nonlocalized and distributed randomly so that there is no systematic relation between the phases of the scattered waves, which could form interference [30].

In the following we consider the problem of light scattering by wood fibre. At first we introduce the basic notations. Then we describe our new Gaussian random shape model for a wood fibre abnd shortly indroduce the geometric optics approximation. To validate the geometric optics approach, we compare the geometric optics and exact results for layered circular cylinders. We compute absorption and scattering cross sections, asymmetry parameters, and the scattering phase matrices using analytical solution for two-layer cylinder and in the geometric optics approximation. We also show comparisons between experimental results for angular scattering measurements of wood-fibre particles and geometric optics calculations.

6.2.1 General aspects

Due to the linearity of the boundary conditions of Maxwell's equations the amplitude of the field scattered by an arbitary single particle is a linear function of the amplitude of the incident field. The relation between incident and scattered field is conveniently described by amplitude scattering matrix [5]

$$\begin{pmatrix} E_{\parallel sca} \\ E_{\perp sca} \end{pmatrix} = \frac{e^{ik(r-z)}}{-ik} \begin{pmatrix} T_2 & T_3 \\ T_4 & T_1 \end{pmatrix} \begin{pmatrix} E_{\parallel inc} \\ E_{\perp inc} \end{pmatrix}. \tag{3}$$

where the complex elements depend general on the scattering and azimuthal angles. The subscripts $\perp$ and $\parallel$ refer to the components of the electric field perpendicular and parallel to the scattering plane, respectively and r is the observer-scatterer distance.

In practice we can analyse radiation by interposing the various polarizer between particle and detector and record the resulting irradiance. It is then more convenient to use the Stokes vector and phase matrix formalism. The properties of light, propagating through a linear medium, are completely described by the Stokes vector $\bar{I} = (I, Q, U, V)^T$

$$
\begin{aligned}
I &= \left\langle E_{\parallel} E_{\parallel}^{*} + E_{\perp} E_{\perp}^{*} \right\rangle \\
Q &= \left\langle E_{\parallel} E_{\parallel}^{*} + E_{\perp} E_{\perp}^{*} \right\rangle \\
U &= \left\langle E_{\parallel} E_{\perp}^{*} + E_{\perp} E_{\parallel}^{*} \right\rangle \\
V &= i\left\langle E_{\parallel} E_{\perp}^{*} - E_{\perp} E_{\parallel}^{*} \right\rangle .
\end{aligned}
$$

where the brackets $\langle\ \rangle$ indicate time averages. Denoting the directions of incidence and scattering by $\Omega_i = (\theta_i, \phi_i)^T$ and $\Omega = (\theta, \phi)^T$, respectively, the Stokes vectors of the incident and scattered light $\bar{I}_i = (I_i, Q_i, U_i, V_i)^T$ and $\bar{I}_s = (I_s, Q_s, U_s, V_s)^T$ are interrelated by the scattering cross section σ_{sca} and the 4x4 scattering phase matrix $\overline{\overline{P}}$,

$$
\begin{aligned}
&\bar{I}_s(\Omega, \Omega_i) = \frac{\sigma_s(\Omega_i)}{4\pi r^{\cdot 2}} \overline{\overline{P}}(\Omega, \Omega_i) \cdot \bar{I}_i(\Omega_i), \\
&\int_{(4\pi)} \frac{d\Omega}{4\pi} P_{11}(\Omega, \Omega_i) = 1
\end{aligned}
\tag{4}
$$

The phase matrix element P_{11} is called scattering phase function. The term phase matrix is inhereted from the field of astronomy and is not related to the phase in the signal sense at all. The relation between the elements of amplitude scattering matrix and scattering matrix can be found for example in [5].
The asymmetry parameter g and the single-particle albedo ϖ are important auxiliary parameters,

$$
\begin{aligned}
g(\Omega_i) &= \int_{(4\pi)} \frac{d\Omega}{4\pi} \cos\theta\, P_{11}(\Omega, \Omega_i), \\
\varpi(\Omega_i) &= \frac{\sigma_{sca}(\Omega_i)}{\sigma_{ext}(\Omega_i)},
\end{aligned}
\tag{5}
$$

where θ is the common, polar scattering angle, and σ_{ext} extingtion cross section, which is a sum of scattering and absorption cross sections

$$
\sigma_{ext} = \sigma_{sca} + \sigma_{abs} .
$$

Albedo is related to the absorption properties of the particle. A particle that scatters all the incident radiation has a zero absorption cross section and an albedo one. A particle that absorbs all the incident radiation is called black-body, but a black-body that is large compared to wavelength has an albedo ½. This is a consequence of including diffraction in the scattering pattern [30]. In the geometric optics approximation the albedo is

$$\varpi = 1/2(1+\varpi^G).$$

The geometric optics part of the albedo ϖ^G for a large black-body is zero
The asymmetry parameter is the first moment of the phase function and describes the average direction of the scattered light. Its values are between 1 and -1. For particles that scatters light isotropically (i.e. the same in all directions) the asymmetry parameter is zero. If the particle scatters more light towards the forward direction (θ=0°) the asymmetry parameter is positive. The asymmetry parameter is negative if the scattering is directed more towards the back direction (θ=180°).

By knowing only the scattering-cross-section-weighted-average asymmetry parameter and albedo of the particles, we can approximate the light scattering properties of the collections of particles reasonably well.

6.2.2 Gaussian random wood fibre model

Barely do wood fibres have shapes of smooth circular cylinders. We have modelled the irregular overall shape and the cell-wall thickness by using state-of-the art statistical methods, Gaussian random cylinders [VIII].

The Gaussian cylinder is described by the covariance function, conveniently modeled by three statistical parameters: the standard deviation of the radius and the correlation lengths of the azimuthal and axial variations. In order to model the cell-wall properly, we assume that the inner boundary is that of a Gaussian random cylinder, and model the outer boundary as an independent lognormal process superimposed upon the inner boundary [IX]. We have altogether eight parameters in our wood-fibre model: the mean (a_L), relative standard deviation (σ_L), correlation angle ($\Gamma_{\varphi,L}$) and axial correlation length ($\ell_{z,L}$) of the fibre lumen, and the corresponding parameters of the fibre cell thickness (a_C, σ_C, $\Gamma_{\varphi,C}$, $\ell_{z,C}$). These parameters characterize the principal geometric factors of the wood fibre. Due to the length-to-diameter ratio of the fibre being always much greater than 5:1, we assume the wood-fibre particles to be infinitely long. As an example, cross-sections of realisations of Gaussian random fibre models are shown in FIGURE 22.

In modelling the complicated cell-wall structure (FIGURE 4), we assume the cell-wall to be an optically homogeneous mixture of holocellulose and lignin. Such a simplifying assumptions can be partly checked against theoretical and experimental results.

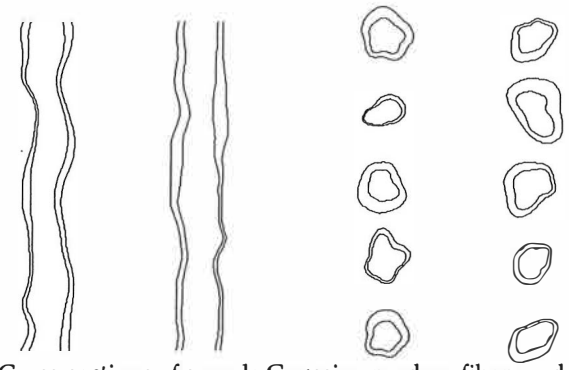

FIGURE 22. Cross-sections of sample Gaussian random fiber model [IX].

The mean volume $\tilde{V}_z$ and the mean surface area $\tilde{A}_z$ of the wood fibre can be estimated by (per unit axial length) [IX].

$$\tilde{V}_z = \pi\tilde{a}_F^2(1+\tilde{\sigma}_F^2) - \pi a_L^2(1+\sigma_L^2), \tag{6}$$

$$\begin{aligned}\tilde{A}_z = {} & 2\pi\tilde{a}_F\left\{1+\tfrac{1}{2}\left[\tilde{\chi}_{\varphi,F}^2+\tilde{\chi}_{z,F}^2\tilde{a}_F^2\exp(3\tilde{\beta}_F^2)\right]-\right.\\ & \tfrac{1}{8}\left[3\tilde{\chi}_{\varphi,F}^4+3\tilde{\chi}_{z,F}^4\tilde{a}_F^4\exp(10\tilde{\beta}_F^2)+2\tilde{\chi}_{\varphi,F}^2\tilde{\chi}_{z,F}^2\tilde{a}_F^2\exp(3\tilde{\beta}_F^2)\right]\\ & \left.+0(\tilde{\chi}^6)\right\},\end{aligned} \tag{7}$$

where standard deviations of the slopes of outer surfaces can be written into the form [IX]

$$\begin{aligned}\tilde{\chi}_{\varphi,F}^2 &= \frac{\upsilon_1\upsilon_2}{\ell_{\varphi,L}^2}+\frac{\upsilon_3}{\ell_{\varphi,C}^2},\\ \tilde{\chi}_{z,F}^2 &= \frac{\upsilon_1\upsilon_2}{\ell_{z,L}^2}+\frac{\upsilon_3}{\ell_{z,C}^2}.\end{aligned} \tag{8}$$

Above we have introduced the variables

$$\begin{aligned}\upsilon_1 &= \ln\left[1+\frac{\tilde{a}_F^2}{a_L^2}\tilde{\sigma}_F^2-\left(\frac{\tilde{a}_F}{a_L}-1\right)^2\sigma_C^2\right]\\ \upsilon_2 &= \frac{a_L^2}{\tilde{a}_F^2}\frac{1+\frac{\tilde{a}_F^2}{a_L^2}\tilde{\sigma}_F^2-\left(\frac{\tilde{a}_F}{a_L}-1\right)^2\sigma_C^2}{1+\tilde{\sigma}_F^2},\\ \upsilon_3 &= \left(1-\frac{a_L}{\tilde{a}_F}\right)^2\frac{1+\sigma_C^2\ln\left(1+\sigma_C^2\right)}{1+\tilde{\sigma}_F^2},\end{aligned} \tag{9}$$

and used equation $\beta_F^2 = \ln(\sigma_F^2+1)$ [XI].

6.2.3 Analytical calculations

The classical way to calculate the elements of the samplitude scattering matrix is the separation of variables in the wave equation (Helmholtz equation). This method can be applied to particles whose boundaries coincide with constant-

coordinate surfaces of the coordinate systems in which the vector wave equation is separable. The most famous solution is the so called Mie scattering [56] for spherical particles. Lord Raleigh [74] and van Ignatowsky [31] solved independently electromagnetic scattering by an infinitely long circular cylinder for perpendicular incidence, arbitary radius and arbitary refractive index. Others have extended the solution to a wider class of infinite cylinders: parabolic cylinders, elliptic cylinders, oblique oriented elliptic cylinders and oblique oriented circular cylinders with a radially inhomogeneous refraction index (see review in [30]).

The complete analytical solution to the problem of layered cylinders for normal incidence (FIGURE 23) has been derived by Kerker and Matijevic [41] who shows how the solution can be extended to any number of layers in cylinder. We have formulated the solution into a form of two sets of linear equations and made a computer program that solves these equations for one to fifty-layer cylinders.

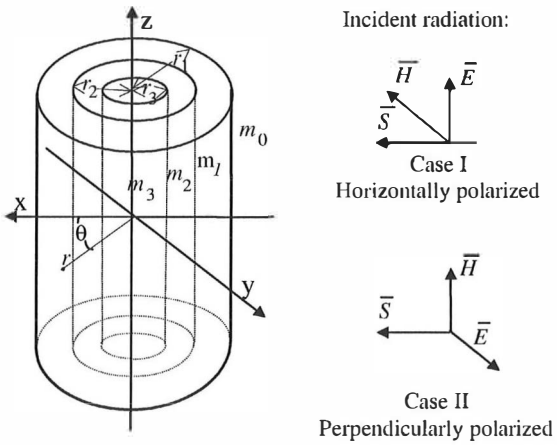

FIGURE 23. Coordinates and vectors for scattering by concentric cylinders; r_1, r_2, r_3 are radii of the cylinders, m_0, m_1, m_2, m_3 are the refractive indexes in the indicated regions and $\bar{S}$, $\bar{E}$, and $\bar{H}$ are Poynting's vector, the electric field vector, and the magnetic field vectors, respectively. θ is the scattering angle.

For normal incidence, the following two sets of solutions to the scalar wave equation corresponds to each of the plane-polarised components of the incident wave [41]. An arbitrary elliptical polarised wave may be formed by linear superposition of these two solutions with complex coefficients.

Case I. $\overline{E}$ parallel to the Cylinder Axis

$$
\begin{aligned}
u &= \sum_{n=-\infty}^{\infty} F_n\left[J_n(m_0 kr) - b_n^0 H_n(m_0 kr)\right] && (r > r_1)\\
u &= \sum_{n=-\infty}^{\infty} F_n\left[B_n^j J_n(m_j kr) - b_n^j H_n(m_j kr)\right] && (r_K > r > r_1)\\
u &= \sum_{n=-\infty}^{\infty} F_n\left[B_n^K J_n(m_K kr)\right] && (r < r_K)
\end{aligned}
\qquad (10)
$$

Case II. $\overline{H}$ parallel to the Cylinder Axis

$$
\begin{aligned}
v &= \sum_{n=-\infty}^{\infty} F_n\left[J_n(m_0 kr) - a_n^0 H_n(m_0 kr)\right] && (r > r_1)\\
v &= \sum_{n=-\infty}^{\infty} F_n\left[A_n^j J_n(m_j kr) - a_n^j H_n(m_j kr)\right] && (r_K > r > r_1)\\
v &= \sum_{n=-\infty}^{\infty} F_n\left[A_n^K J_n(m_K kr)\right] && (r < r_K)
\end{aligned}
\qquad (11)
$$

The Hankel function of the first kind, $H_n(z)$ is defined by

$$H_n(z) = J_n(z) + iN_n(z),$$

where $J_n(z)$ and $N_n(z)$ are the Bessel functions of the first and the second kinds, respectively. The F_n term is defined by

$$F_n = (-1)^n e^{in\theta + i\omega t},$$

where $\omega/2\pi$ is the frequency and t is time; $k = 2\pi/\lambda$ is the wave number, and $a_n^j, A_n^j, b_n^j, B_n^j$ are unknown coefficients.

The boundary conditions require that mu, $m\partial u/\partial r$, $m^2 v$ and $\partial v/\partial r$ are continuous. By applying the boundary conditions and solutions (10) (11) we can formulate the problem in the form of systems of two linear equations. Below we present these systems of equations for the case of a three-layer cylinder (FIGURE 23):

$$
\begin{bmatrix}
m_0 H_n(m_0\alpha_1) & -m_1 H_n(m_1\alpha_1) & m_1 J_n(m_1\alpha_1) & 0 & 0 & 0\\
m_0^2 H_n'(m_0\alpha_1) & -m_1^2 H_n'(m_1\alpha_1) & m_1^2 J_n'(m_1\alpha_1) & 0 & 0 & 0\\
0 & -m_1 H_n(m_1\alpha_1) & m_1 J_n(m_1\alpha_2) & m_2 H_n(m_2\alpha_2) & -m_2 J_n(m_2\alpha_2) & 0\\
0 & -m_1^2 H_n'(m_1\alpha_1) & m_1^2 J_n'(m_1\alpha_2) & m_2^2 H_n'(m_2\alpha_2) & -m_2^2 J_n'(m_2\alpha_2) & 0\\
0 & 0 & 0 & m_2 H_n(m_2\alpha_3) & -m_2 J_n(m_2\alpha_3) & m_3 J_n(m_3\alpha_3)\\
0 & 0 & 0 & m_2^2 H_n'(m_2\alpha_3) & -m_2^2 J_n'(m_2\alpha_3) & m_3^3 J_n'(m_3\alpha_3)
\end{bmatrix}
\begin{bmatrix} b_n^0\\ b_n^1\\ B_b^1\\ b_n^2\\ B_n^2\\ B_n^3 \end{bmatrix}
=
\begin{bmatrix} m_0^2 J_n(m_0\alpha_1)\\ m_0 J_n'(m_0\alpha_1)\\ 0\\ 0\\ 0\\ 0 \end{bmatrix}
$$

$$\begin{bmatrix} m_0^2 H_n(m_0\alpha_1) & -m_1^2 H_n(m_1\alpha_1) & m_1^2 J_n(m_1\alpha_1) & 0 & 0 & 0 \\ m_0 H_n'(m_0\alpha_1) & -m_1 H_n'(m_1\alpha_1) & m_1 J_n'(m_1\alpha_1) & 0 & 0 & 0 \\ 0 & -m_1^2 H_n(m_1\alpha_1) & m_1^2 J_n(m_1\alpha_2) & m_2^2 H_n(m_2\alpha_2) & -m_2^2 J_n(m_2\alpha_2) & 0 \\ 0 & -m_1 H_n'(m_1\alpha_1) & m_1 J_n'(m_1\alpha_2) & m_2 H_n'(m_2\alpha_2) & -m_2 J_n'(m_2\alpha_2) & 0 \\ 0 & 0 & 0 & m_2^2 H_n(m_2\alpha_3) & -m_2^2 J_n(m_2\alpha_3) & m_3^2 J_n(m_3\alpha_3) \\ 0 & 0 & 0 & m_2 H_n'(m_2\alpha_3) & -m_2 J_n'(m_2\alpha_3) & m_3 J_n'(m_3\alpha_3) \end{bmatrix} \begin{bmatrix} a_n^0 \\ a_n^1 \\ A_n^1 \\ a_n^2 \\ A_n^2 \\ A_n^3 \end{bmatrix} = \begin{bmatrix} m_0^2 J_n(m_0\alpha_1) \\ m_0 J_n'(m_0\alpha_1) \\ 0 \\ 0 \\ 0 \\ 0 \end{bmatrix}$$

where the primes denote derivatives with respect to r and $\alpha_j = kr_j$.

We used IMSL subroutines DCBYS and DBSJNS to calculate the values of complex Bessel functions and subroutine DLSACG to solve the above systems of linear equations for unknown complex coefficients $a_n^j, A_n^j, b_n^j, B_n^j$, $(j = 0,1,2,3)$. For normal incidence the amplitude scattering matrix (3) for infinite circular cylinder reduces into the form [5]

$$\begin{bmatrix} T_1(\theta) & 0 \\ 0 & T_2(\theta) \end{bmatrix}$$

The elements of the amplitude scattering matrix $T_1(\theta)$ and $T_2(\theta)$ corresponding to the case I and case II respectively, can be calculated using the formulas [5]

$$T_1(\theta) = \sum_{n=-\infty}^{\infty} b_n^0 e^{in\theta} = b_n^0 + 2\sum_{n=1}^{\infty} b_n^0 \cos(n\theta)$$

$$T_2(\theta) = \sum_{n=-\infty}^{\infty} a_n^0 e^{in\theta} = a_n^0 + 2\sum_{n=1}^{\infty} a_n^0 \cos(n\theta).$$

Only the coefficients of positive order are needed because:

$$b_n^0 = b_{-n}^0, \quad a_n^0 = a_{-n}^0.$$

The extinction efficiency, Q_{Ext}, and the and scattering efficiency, Q_{Sca}, are defined in the usual way as the corresponding cross section per unit length divided by $2r_1$, the diameter of the cylinder. For finite cylinder of length L and radius r_1, Q is the ratio between the cross section and the normally projected geometric area of the cylinder, $2r_1 L$.

The extinction efficiencies are obtained by using the optical theorem and the scattering efficiencies are obtained by integrating the differential cross section. For perpendicular incidence these can be written in the following form [5]:

$$Q_{Ext,I} = \frac{C_{Ext,I}}{2r_1} = \frac{2}{kr_1}\mathrm{Re}\left\{b_0^0 + 2\sum_{n=1}^{\infty}\left|b_n^0\right|\right\} = \frac{2}{x}\mathrm{Re}(T_1(\theta = 0))$$

$$Q_{Sca,I} = \frac{c_{Sca,I}}{2r_1} = \frac{2}{kr_1}\left[\left|b_0^0\right|^2 + 2\sum_{n=1}^{\infty}\left(\left|b_n^0\right|^2\right)\right]$$

$$Q_{Ext,II} = \frac{c_{Ext,II}}{2r_1} = \frac{2}{kr_1}\mathrm{Re}\left\{a_0^0 + 2\sum_{n=1}^{\infty}\left|a_n^0\right|\right\} = \frac{2}{x}\mathrm{Re}(T_2(\theta = 0))$$

$$Q_{Sca,II} = \frac{c_{Sca,II}}{2r_1} = \frac{2}{kr_1}\left[\left|a_0^0\right|^2 + 2\sum_{n=1}^{\infty}\left(\left|a_n^0\right|^2\right)\right].$$

If the incident light is unpolarised, the efficiencies are:

$$Q_{Ext} = \frac{1}{2}(Q_{Ext,I} + Q_{Ext,II}), \quad Q_{Sca} = \frac{1}{2}(Q_{Sca,I} + Q_{Sca,II}).$$

We studied the effects of radius of the lumen, cell-wall thickness, and standard deviation of cell-wall thickness on the albedo using the analytical solution for the two-layer circular cylinder. Radius of the lumen and cell-wall thickness were random variables with lognormal distributions. We calculated average single particle albedos for 75 cases with different sets of parameters (Table 13), using 10 000 realization for each case. FIGURE 24 a) shows albedos of 15 cases, which all have the same refraction index and wavelengths, as funtions of mean cell-wall volume per axial length. Albedo is not a simple function of mean cell-wall volume, but a radius of the lumen has a great effect on it. FIGURE 24 shows an interesting result, when cell-wall volume is devided by radius of lumen. Based on this result we developed an empirical formula for single scattering albedo

$$\varpi^e = 1 - 3.33\frac{k}{\lambda n}\frac{V_z}{a_L} + 20\left(\frac{k}{\lambda n}\frac{V_z}{a_L}\right)^2. \tag{12}$$

where

$$V_z = \pi a_F^2 \sigma_F^2 - \pi a_L^2 \sigma_L^2.$$

In FIGURE 25 we compare the results of the above mentioned 75 cases calculated by analytical method and results given by empirical formula (12).

TABLE 13. Parameters for two-layer cylinder albedo calculations. Three different inner radiuses (10 μm, 15 μm, 20 μm) and five different cell-wall thicknesses (2 μm, 3 μm, 4 μm, 5 μm, 6 μm) was used for each parameter combination i.e. totally 75 cases. Standard deviation of the lumen was 2 μm in each case. $a_c\sigma_c$ is standard deviation of cell-wall thickness. The complex refraction index for cell-wall is m=n+ik.

Set number	λ [μm]	n	k	$a_c\sigma_c$	Symbol in Fig. 25
1	1.20	1.7	0.0001	2	x
2	1.44	1.5	0.0004	2	+
3	1.44	1.3	0.0004	2	o
4	1.44	1.5	0.0004	3	□
5	1.93	1.5	0.0020	2	◊

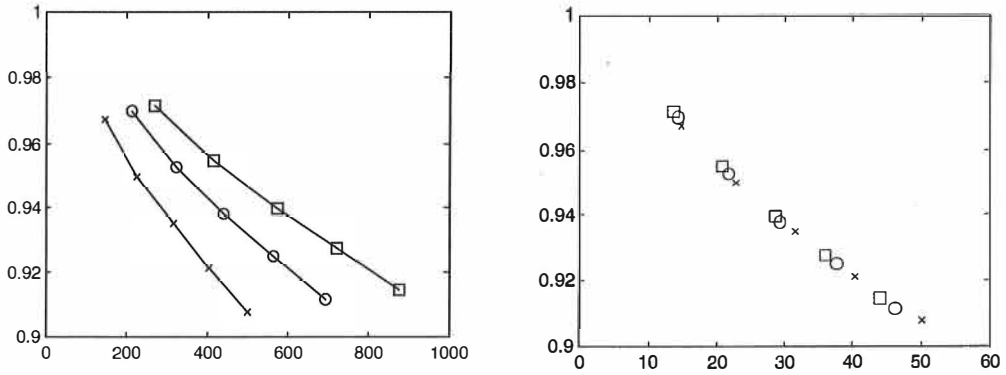

a) b)

FIGURE 24. Single-particle albedos of two-layer cylinders for normal incidence. In figure a) albedos vs. V_z . In figure b) albedos vs. V_z / a_L . Mean radius of the lumen (i.e. inner radius of the cylinder) a_L is 'x' =10 μm, 'o'=15 μm, and '□' = 20 μm. Refraction index of the cell-wall is 1.5+0.002i and wave length 1.93 μm, V_z is the mean volume of the cell-wall per axial unit length.

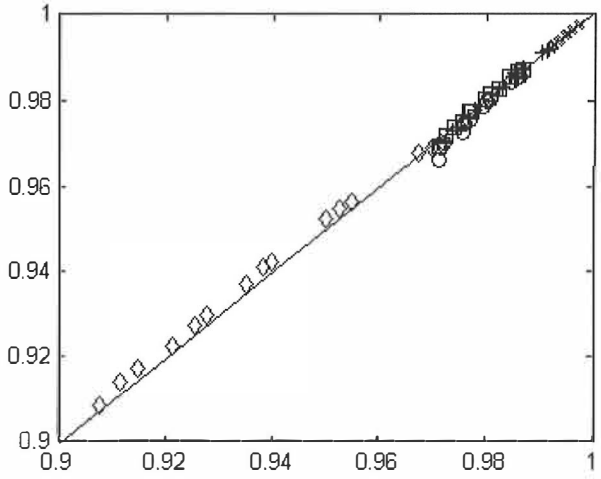

FIGURE 25. Comparison between the single-particle albedos calculated by analytical solution for two-layer infinite cylinder for normal incidence and albedos calculated by equation (12). Parameters are in Table 14. (dotted line) [IX]

6.2.4 Geometric optics approximation

The non-smooth shape of the realistic wood fibre does not conform to a single coordinate system and thus the wave equation becomes extremely difficult to solve. On the other hand the wood fibre is so large compared to wavelength of NIR radiation that the computations using numerical methods like discrete dipole approximation [72] are very time consuming even with modern super-computers.

Geometric optics (GO) together with Fraunhofer diffraction (GO method, e.g., Muinonen et al. 1996 [65]) can be applied to practicaly arbitary any particle shapes. It is based on the assumption that the incident plane wave can be represented as a collection of independent and parallel rays. The history of each ray reflecting or refracting on the particle surfaces is traced using Snell law and Fresnel's equations (e.g. [5]). The sampling of all escaping rays into predifined angular bins supplemented by the computation of Fraunhofer diffraction of the incident wave on the particle projection yields a quantitative representation of the scattering properties of the particle. The disadvantage of the GO method is that it is only applicable to scatterers that are large enough compared to wavelength, thus its applicability in terms of smallest particle size must be checked by comparing the results against exact analytical or numerical solutions.

We have developed geometric optics approximation that calculates the whole scattering matrix for the Gaussian random cylinder [VIII] and for the Gaussian random wood-fibre model [IX].

Based on the new wood-fibre model and geometrics optics approximation, we have developed a new graphic parameter estimation method for retrieving information about wood-fibres from measurements. For the light scattering

measurements we used an angular scatterometer located at the Institute of Technical Thermodynamics, Stuttgart [IX].

The results are summarized in FIGURE 26 and in TABLE 14. Sample Gaussian random wood-fibres generated with 'best fit' parameters are presented in FIGURE 22. FIGURE 26 shows the normalized projected-area-weighted mean-scattering phase function (solid curve) for the entirely set of measurements together with geometric optics results for the best-fit Gaussian fibre model (dotted ciurve). The agreement of these two curves is good.

TABLE 14. Shape parameters [IX]

Notation	Name	Literature [43]	Measured	'best fit' – parameters
a_F	Mean radius of the fibre [μm]	19.4	14.7	14.7
a_L	Mean radius of the lumen [μm]			10.7
a_C	Mean cell thickness [μm]	4.8		4.0
$\bar{d}\sigma_d$	Standard deviation of the diameter of the fibre [μm]	7.0	4.6	
$a_F\sigma_F$	Standard deviation of the radius of the fibre [μm]			3.2
$a_L\sigma_L$	Standard deviation of the radius of the lumen [μm]			2.5
$a_C\sigma_C$	Standard deviation of the cell wall thickness [μm]	2.2		2.0
$\Gamma_{\varphi,L}$	Azimuthal correlation angle of the lumen [°]			28
$\Gamma_{\varphi,C}$	Azimuthal correlation angle of the cell [°]			90
$\ell_{z,L}$	Axial correlation length of the lumen			1
$\ell_{z,C}$	Axial correlation length of the cell			3

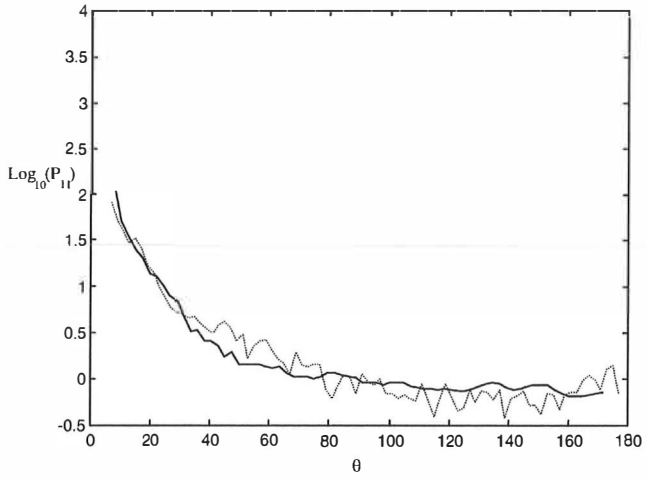

FIGURE 26. Comparison of the projected-area-weighted mean scattering phase function of the entire set of measurements (solid line) and simulated phase function with the 'best fit' parameters in TABLE 14. (dotted line) [IX]

Takano and Tanaka [96] presented the first detailed comparison between geometric optics approximation and analytical solution for infinite solid circular cylinder. In FIGURE 27 and in TABLE 15 we present the first comparison between the analytical and geometric optics solution for infinite two-layer circular cylinder. Absorption band of water with the extinction koefficients k of water was selected as one test band and an other band in the area where the absorption to the water is smalle. Albedos are allmost the same and the over all agreement of the phase functions is quite good, however there is a small difference around the scattering angle of 50 degrees. We conclude that geometric optics is a good approximation method for wood fibre size particles, although cell-wall thickness is not very large compared to the wavelength in NIR region.

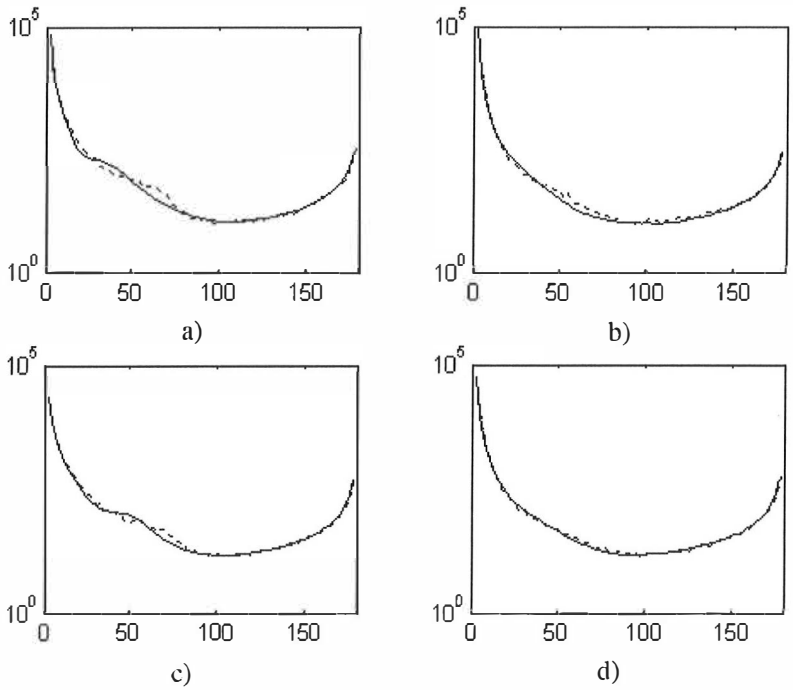

FIGURE 27. Comparion of the logarithmic phase functions, Log(P_{11}), for infinite two-layer circular cylinders as functions of scattering angle. Solid line analytical solution, dotted line geometric optics approximation. Parameters for cases in a), b), c), and d) are presented in TABLE 15.

TABLE 15. Comparison of single scattering albedos for infinite two-layer circular cylinder. ϖ is analytical solution, $1/2(1+\varpi^G)$ is geometric optics approximation. m=n+ik is the complex refraction index for cell-wall

Case	a	a	λ	n	k	ϖ	$1/2(1+\varpi^G)$
a	10	15	1.93	1.5	0.0020	0.9213	0.9265
b	10	12	1.93	1.5	0.0020	0.9674	0.9686
c	10	15	1.20	1.7	0.0001	0.9931	0.9938
d	10	12	1.20	1.7	0.0001	0.9971	0.9974

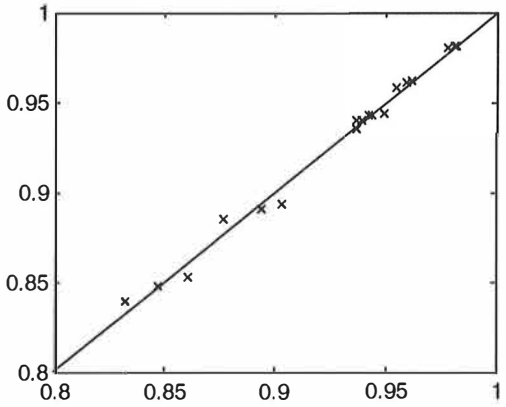

FIGURE 28. Comparison between the albedos calculated for randomly oriented Gaussian random wood fibre model by geometric optics approximation and the albedos calculated by equation (13). Parameter set 3 and 5 in TABLE 13 was used for three different inner radiuses (10 μm, 15 μm, 20 μm) and three different cell-wall thicknesses (2 μm, 4 μm, 6 μm) i.e. totally 18 cases. Other shape parameters are the best-fit parameters in TABLE 14.

The albedo of the randomly oriented Gaussian random wood fibre model can also be estimated quite well with a similar kind of formula like (12) (FIGURE 28)

$$\varpi^G = 1 - 6.5\frac{k}{\lambda n}\frac{V_z}{a_L} + 55\left(\frac{k}{\lambda n}\frac{V_z}{a_L}\right)^2. \qquad (13)$$

The mean cell-wall volume (6) can be written into the following formula

$$V_z = \pi\left[2a_L a_c + a_c^2(1+\sigma_c^2)\right],$$

which shows that the cell-wall thickness has a strong effect on the albedo.

The effects of correlation angles and correlation lengths on the albedo and asymmetry parameter of randomly oriented Gaussian random wood fibre model are shown in Tables 16, 17, and, 18 in geometric optics approximation for a_c = 4 μm, a_L=10 μm , $\sigma_c a_c$=2.0 μm, $\sigma_L a_L$=2.3 μm λ=1.44 μm, and refraction

index m=1.5+0.0004i. In general albedo is fairly insensitive to the changes in statistical parameter, varying between 0.955 and 0.963, so that larger values correspond to larger correlation lengths and correlation angles. Asymmetry parameter behaves in a similar way. For smoother wood fibre the asymmetry parameter is larger.

TABLE 16. The geometric optics single-particle albedos ϖ and asymmetry parameters g (Eg. (5)) for randomly oriented wood fibre model , λ=1.44 μm , m=1.5+0.0004i, $\Gamma_{\varphi,L}$ = 30, and $\ell_{z,L}$=1 as a function of azimuthal correlation angle of cell-wall $\Gamma_{\varphi,C}$ and axial correlation length of cell-wall $\ell_{z,C}$

$\Gamma_{\varphi,C}$	$\ell_{z,C}$=1		$\ell_{z,C}$=3	
	ϖ	g	ϖ	g
30	0.955	0.866	0.955	0.884
60	0.956	0.875	0.955	0.891
90	0.956	0.881	0.956	0.895

TABLE 17. The geometric optics single-particle albedos ϖ and asymmetry parameters g (Eg. (5)) for randomly oriented wood fibre model , λ=1.44 μm , m=1.5+0.0004i, $\Gamma_{\varphi,L}$ = 30, and $\ell_{z,L}$=1 as a function of azimuthal correlation angle of cell-wall $\Gamma_{\varphi,C}$ and axial correlation length of cell-wall $\ell_{z,C}$ $\ell_{z,C}$

$\Gamma_{\varphi,C}$	$\ell_{z,C}$=1		$\ell_{z,C}$=3	
	ϖ	g	ϖ	g
30	0.955	0.885	0.955	0.905
60	0.955	0.912	0.960	0.923
90	0.957	0.907	0.963	0.929

TABLE 18. The geometric optics single-particle albedos ϖ and asymmetry parameters g (Eg. (5)) for randomly oriented wood fibre model , λ=1.44 μm , m=1.5+0.0004i, $\Gamma_{\varphi,C}$ = 90, and $\ell_{z,C}$=3 as a function of azimuthal correlation angle of lumen $\Gamma_{\varphi,L}$ and axial correlation length of lumen $\ell_{z,L}$

$\Gamma_{\varphi,L}$	$\ell_{z,L}$=1		$\ell_{z,L}$=3	
	ϖ	g	ϖ	g
30	0.956	0.895	0.958	0.913
60	0.955	0.912	0.961	0.927
90	0.957	0.916	0.963	0.929

7 CONCLUSIONS

We have considered near infra-red measurements and control systems for thermomechanical refiners. The new contribution of this work can be summarised as follows.

We have shown that the consistency of TMP pulp can be measured accurately in the blow line of the refiner by the NIR technique with the PCR calibration method. Moreover we have developed a new adaptive refiner control systems based on consistency measurements.

More than 90 systems have been installed around the world with excellent results. Consistency variations have decreased by 50 to 80 percent and variations in refiner motor loads by 30 to 70 percent. This results in a simultaneous decreasement of variations in specific energy and refining intensity and thus a much more even pulp quality. Freeness, fibrelength, tear and tensile index, variations have decreased up to 80%.

The common argument is that with the NIR-technique we measure the chemical composition of the measurement object. However, we have shown using statistical methods that there is good correlation between the measured spectra and the pulp properties, which should not depend on the chemical properties of the fibres, such as the Canadian standard freeness and the fibre size distributions.

In order to understand the interaction between NIR radiation and the pulp particles, we have developed a new model for the random shape of the hollow wood fibre particle using multivariate lognormal statistics. This model together with the geometric optics treatment explains the scattering measurements of a single wood fibre in an excellent way.

Based on introduced theoretical modelling, we have developed a new method for retrieving physical information on wood fibres from measurements of their light scattering characteristics, in particular, the scattering phase functions and degrees of linear polarizations.

Due to absorption in the NIR –region, albedo of the average pulp particle has a dominant effect the on reflectance spectra of pulp. We have shown using theoretical methods that albedo depends greatly on cell-wall thickness, which

mainly defines the flexibility of the fibre. Also other shape parameters of the fibre have effects on albedo and the asymmetry parameter as well. Thus we claim that when we are measuring the quality of pulp by the NIR technique, we are mostly defining the shape parameters of the average pulp particle, and not so much their chemical composition.

This is further confirmed by the fact that there has been found a good correlation between values given by image analysis techniques and strength properties of the pulp although the chemical components are not measured by these thechniques.

The relation between the measured spectra and the shape parameters is a complex one, and will be the subject of our later studies. These studies will lead us toward a physical ('hard') calibration model (instead of statistical ('soft') calibration model) with less unknown parameters to estimate. Also better physical understanding will help us to design the experiments so that less calibration samples are needed.

REFERENCES

[1] Allison,B.J., Ciarniello, J., Tessier, P., and Dumont, G.A., Dual adaptive control of chip refiner motor load: industrial results, Pulp and Paper Canada, 96(3), T73-T79(1995)

[2] Antti, H. Multivariate characterization of Wood related materials. Ph.D thesis, University of Umeå (1991).

[3] Atack D. Technical Development of Mechanical Pulping Process Preprint International Mechanical Pulping Conference Stocholm (1985).

[4] Biermann, C.J., Handbook of Pulping and Papermaking,Second edition, Academic Press California (1996).

[5] Bohren C. F., Huffman D. R., Absorption and Scattering of Light by Small Particles, Wiley, New York (1983).

[6] Brill J. W., Effects of Wood and Chip Quality on TMP Properties, Preprint International Mechanical Pulping Conference Stocholm (1985)

[7] Broderick, G., Paris, J., Valade, J.L., and Wood, J.:Applying latent vector analysis to pulp characterization., Paperi ja Puu – Paper and Timber vol. 77:6,7410-418 (1995).

[8] Cameron F., Koivo H. N., Partanen K., Self-tuning Control of Freeness in a Thermomechanical Pulping Plant Report 9-83, Tampere University of Technology (1983)

[9] Carlsson, J., Persson, W., Hellentin, P., and Malmqvist, L., The Propagation of light in paper: modeling and Monte Carlo simulations, In Proceedings of the 1995 International Paper Physics Confrerence, CPPA, September 11-14, Niagara-on-the-Lake, Canada, 83-86 (1995).

[10] Claudio-da-Silva, E., The flexibility of pulp fibres – a structural approach, Proceedings of International Paper Physics Conference, Harwichport, MA, Sept. 18-22(1983), 13-25.

[11] Cort, J.B., Keller, W.F., Larose, L._P., and Goulet, M., Automass Control Results in More Uniform Pulp Quality at Daishova Inc. Quebec city, 78th CPPA Annual Meeting, Montreal, B165-171(1992)

[12] Cutler, C.L., and Ramaker, B.L., Joint Automatic Control Conference, American Automation Control Council, Green Valley Ariz., 1980, Paper WP5-B.

[13] Dahlquist, G. and Ferrari, B., Mill operation experience with a TMP refiner control based on a true disc clearence measurement. International Mechanical Pulping Conference Session III:n:o 6, Oslo 1981, 1-14

[14] Dahlin G., Hill J., Automatic quality control of TMP manufacture, Appita 32 (1979)

[15] Dodson, C.T.J.,The effect of fibre length distribution on Formation, Journal of Pulp and Paper Science Vol 18(2),1992,J74-J76

[17] Dumont, G.A., Legault, N.D., and Rogers, J.H.,Computer control of TMP plant, Preprint International Mechanical Pulping Conference, Session III n:o 1,Oslo 1981,1-19

[18] Dumont G. A., Self tuning control of the chip refiner motor load Automatica 18 (1982)
[19] Frazier W., Applying hydrodynamic bearing theory to the refiner plate–pulp fibre interaction Preprint International Mechanical Pulping Conference Stocholm (1985)
[20] Forgacs O. L., The characterization of mechanical pulps, Pulp and Paper Magazine of Canada 64(1963):C T89 - T118
[21] Fournier, M.Pa., H., Shallhorn, P.M., and Roche, A.A., Control of Chip refining Operations, Proceedings of International Mechanical Pulping Conference, Minneapolis, 91-100(1991)
[22] Gustavson, I., Ljung, L., and Söderström, T. "Identification of Processes in Closed Loop – Identifiability and Accuracy Aspects", Automatica, Vol 13(1977) 59-75.
[23] Haario, H.and Taavitsainen, V.-M., Data Analysis Toolbox for use with MATLAB, User's guide, Control Cad OY, Espoo (1991).
[24] Heikkurinen A., Levlin J., Paulapuro H., Principles and methods in pulp characterization - Basic fibre properties, Paperi ja Puu 73:5(1991), 411-417.
[25] Helland, I.S., Partial Least Squares Regression and Statistical Methods. Scandinavian Journal of Statistics, 17, 97-114 (1990)
[26] Hill J., Westin H., Bergström R., Monitoring pulp quality for process control purposes Preprint International Mechanical Pulping Conference Toronto (1979)
[27] Hill J.,Control systems for mechanical pulp improve quality, plant operations Pulp & Paper July 1981
[28] Hill J., Process understanding profits from sensor and control developments Preprint International Mechanical Pulping Conference Oslo (1993)
[29] Honkasalo J.V., Pölkkynen E. E., Vainio J. A., Development of Control Systems in Mechanical Pulping (GW, TMP) Preprint International Mechanical Pulping Conference Helsinki (1989)
[30] van de Hulst, H.C. "Light Scattering by Small Particles," (Wiley, New York, 1957).
[31] von Ignatowsky, W., Reflexion elektromagnetischer Wellen an einem Draht, Ann.Phys. 18, 495-522 (1905).
[32] Ilvessalo-Pläfli,M.-S., Puun rakenne; Puukemia, Suomen Paperi-insinööri yhdistyksen käsikirja (Jensen, W. ed.) Turku (1977)
[33] Johnsen, P.O., Skinnarland, L., Helle, T., and Housen, P.J. Distribution of lignin and other material on particle surfaces in mechanical pulp. In Proceedings of the International Mechanical Pulping Conference, (Ottawa 1995).
[34] Jordan, B.D., Page, D.H., Application of image analysis to pulp fibre characterization: Part I, Proceedings of International Paper Physics Conference, Harrison, Hot Springs, B.C. Sept. 17-19 (1979), 105-114.
[35] Jolliffe, I.T., Principal Component Analysis. Springer-Verlag New York (1986)

[36] Joutila, P. Modelling of TMP line. Diploma thesis. Tampere University of Tecnology, 1987.
[37] Kano, T., Iwamida, T., and Sumi, Y. Energy Consumption in Mechanical Pulping. Pulp Paper Can. 83(6) 1982, T157-T161.
[38] Karaila, I., Modeling of Fibre Concentration in Pulp Suspensions, Ph.D thesis, Tampere University of Technology, Publications 232 (1998).
[39] Karnis, A., The mechanism of fibre development in mechanical pulping. Journal of Pulp and Paper Science 20:10,(1994), J280-J288.
[40] Kay, S.M., Modern Spectral Estimation, Prentige Hall, New Jersey (1988)
[41] Kerker, M., and Matijevic, E., *JOSA* **51**, 506- (1961).
[42] Klemetti, V. and Nygord, M., Kajaani FSA users manual. Kajaani Elektroniikka Inc., Kajaani 1994
[43] Koljonen, T. and Heikkurinen, A., "Delamination of stiff fibres," In Proceedings of the International Mechanical Pulping Conference, (Ottawa 1995).
[44] Kolmogorov, A.N., Interpolation und Extrapolation von Stationären Zufälligen Folgen, Bull. Acad. Sci. USSR Ser.Math. Vol. 5 (1941)
[45] Kooi S.R.L., Khorosani K., Control of the wood chip refiner using Neural Network, Tappi Journal June (1992)
[46] Kubelka, P. and Munk, F., Ein Beitrag zur Optik der Farbanstriche, Zeitscrhift für technische Physik, 12, 593-601 (1931).
[47] Kuusela R., Infrared Moisture Measurement of Paper, Board and Pulp, Ph.D thesis University of Kuopio (1990)
[48] Leskelä, L.,A model for the optical properties of paper, Paperi ja Puu - Paper and Timber, 75, 683-688 (1993).
[49] Levlin, J-E., On the suitability of the McNett classifier for the fibre-length classification of pulps. Paperi ja Puu – Paper and Timber, 64:4,213-216(1982)
[50] Ljung, L., System Identification: Theory for the User, Prentice-Hall, New Jersey (1987)
[51] Luukko.K and Nurminen, I., Fines generation in the first-stage refiner of thermomechanical pulping. Paperi ja Puu – Paper and Timber vol 81(4)1999, 311-315.
[52] MacDonald J. E., Guthrie J. J., Chip Mass Flow Meter, Preprint International Mechanical Pulping Conference Vancouver (1987)
[53] Martens H., Naes T., Multivariate Calibration, Wiley, Chichester (1989)
[54] McClure, F.W. Near-Infrared Spectroscopy. The Giant is Running Strong. Analytical Chemistry, Vol 66:1 (1994) 43A-53A.
[55] McQueen, S., Cluett,W.R., and Duever, T., Identification of a wood chip refiner with implications for process control.TAPPI Jornal, vol 82:5 1999, 122-129.
[56] Mie G., Beiträge zur Optik trüber Medien, speziell kolloidaler Metallösungen. Ann. Physik. 25/3(1908)
[57] Mihelich W. G., Wild D. J., Beaulieu S. B., Beath L. R., Single-Stage Chip Refining - Some Major Operating Parameters and Their Efects on Pulp Quality, Pulp and Paper Magazine of Canada, 73:5 (1972)

[58] Miles, K.B., Dana, H.R., and May, W.D., The flow of steam in chip refiners. Preprints International Symbosium on Fundamental Concepts of Refining, Appleton, Wisconsin, 30-42 (1980).
[59] Miles K. B., May W. D.,The Flow of Pulp in Chip Refiners, Journal of Pulp and Paper Science, 16(2), J63-J72 (1990).
[60] Miles K. B., Karnis A., The responce of mechanical and chemical pulps to refining Tappi Journal,74(1),157-164(1991)
[61] Miles, K.B., May, W.D., and Karnis, A. Refining intensity, energy consumption, and pulp quality in two-stage chip refining. TAPPI Journal Vol 74(3), 221-230 (1991).
[62] Miles,K.B., A simplified method for calculating the residence time and refining intensity in a chip refiner. Paperi ja Puu – Paper and Timber, 73(9),852-857(1991)
[63] Mohlin, U.-B., Fibre bonding ability a key pulp quality parameter for mechanical pulps to be used in printing papers. Int.Mech. Pulping Conf. June 6-8, Vol 1, Helsinki 1989, 49-57
[64] Montgomery D. C., Statistical Quality Control, Second Edition, John Wiley & Sons, New York (1991)
[65] Muinonen, K., Nousiainen, T., Fast, P. , Lumme, K., and Peltoniemi, J.I. "Light scattering by Gaussian Random particles: ray optics approximation," J. Quant. Spectrosc. Radiat. Transfer , **55**, 577-601 (1996).
[66] Newman B. G., Stationwala M. J., Atack D.Analysis of steam flow in disc refining Preprint International Mechanical Pulping Conference Stocholm (1985)
[67] Paavilainen, L. Influence of fibre morphology and processing on the soft wood sulphate pulp fibre and paper properties. Ph.D thesis, Helsinki University of Technology (1993).
[68] Perkola M., TMP-jauhatuksen teoreettinen tarkastelu, Licentiate Thesis, Tampere University of Technology (1985)
[69] Pietinen P., Savonjousi A.United State Patent 5 016 824. Method and Apparatus for Controlling the Production of Thermomechanical Pulp. Appl. 457 723, 15.7.1988.
[70] Pietinen P., Tiikkaja E., Developments in On-line Analysers for Refiner Contrrol Preprint International Mechanical Pulping Conference, Oslo 44-52 (1993)
[71] Prette, D.M. and Gillette, R.D. "Optimization and and Contrained Multivariable Control of Catalytic Cracking Unit", Proceedings of JACC, 1980.
[72] Purcell, E.M., and Pennypacker, C.R., "Scattering and absorption of light by nonspherical dielectric grains," Astrophys. J. **186**, 705-714 (1973).
[73] Rao C.R., Linear statistical inference and its applications, Second edition, Whiley New ork (1973)
[74] Rayleigh, L., "On the electromagnetic theory of light," Philos.Mag.vol. **12**, 81-101 (1881).

[75] Reme, P.A. and Helle, T. Quantitative Assessment of Mechanical Fibre Dimenions During Defibration and Fibre Development. Journal of Pulp and Paper Science 27(1)2001,1-7.
[76] Richalet, J. A., Rault, A., Testud, J.D., and Papon, Model predictive heuristic control. J., Automatica 14(1978) 413 - 428.
[77] Roche,A., Owen, J., Miles, K., and Harrison, R., A practical approach to the control of TMP refiners. Control System 96,129-135.
[78] Saarinen K., Savonjousi A., Hierteen tiheys- ja kosteussäätöjärjestelmä TERMAP ja hierrinlinjan automatisointi, Paperi ja Puu - Paper and Timber 5 (1989),in Finnish
[79] Saarinen K., TCA Test Runs ,Report, ABB Process Automation, Vaasa (1991)
[80] Saarinen, K. Measurement of Consistency of Thermo-Mechanical Pulp in the Blow line of the Refiner by the Infra-Red Method. University of Jyväskylä, M.Sc thesis, Department of Physics (1993).
[81] Saarinen K., Method and apparatus for determining of refiner mechanical pulp freeness, *Finish Patent 91446*(1993)
[82] Saarinen K, Consistency Measurement Based Adaptive Control System for Thermo Mechanical Refiners, Licentiate thesis, University of Jyväskylä, Department of Mathematics, Jyväskylä (1993)
[83] Saarinen K., Orkisz M.Method for determination of rotation speed, Finish Patent 20000646 (2001)
[84] Saarinen K., Orkisz M Method for determination of rotation speed of the induction motor, Finish Patent 20000647 (2001)
[85] Saarinen K., Korendo Z, A method for technical condition assessment of rotating machines and electrical motors in particular, Polish Patent 338286 (2001)
[86] Sköld, H. and Nilson, P., PQM1000 fibre and shive classifier based on image analysis, Preprint , International Mechanical Pulping Conference, Oslo 1993.
[87] Stationwala M. I., Atack D., Wood J. R., Wild D.,J., Karnis A.,The effect of control variables on refining zone conditions and pulp properties, Paperi ja Puu 73(1991):1
[88] Stationwala, M.I., Mathieu, J., and Karnis, A. On the interaction of wood and mechanical pulping equipment. Part I:fibre development and generation of fines. Journal of Pulp and Paper Science 22(1996):5, J155-J160.
[89] Stationwala, M.I., Mathieu, J., and Karnis, A. On the interaction of wood and mechanical pulping equipment. Part II: Pulp quality. Proceedings of International Mechanical Pulping Conference, Ottawa, 165-170 (1995)
[90] Stone, M. and Brooks, R.J., Continuum Regression: Cross-validated Sequentially Constructed Prediction Embracing Ordinary Least Squares, Partial Least Squares and Principal Components Rgeression. Journal of the Royal Statistical Society, B 237-269 (1990)

[91] Strand B. C., Hartler N., Modelling and Optimization of Full Scale Chip Refining, Preprint International Mechanical Pulping Conference, Stocholm 46-54 (1985).
[92] Strand, W.C., Simulation, Control and on-line optimization of mechanical pulping systems, Ph.D thesis, University of Idaho 1989.
[93] Strand W. C., Ferritus O., Mokvist A. V., Use of Simulation models in the on line Control and Optimization of the Refining Process Tappi Journal November (1991)
[94] Strand, B.C., Mokvist, A., Sköld, H., Ferritsius, O., and Jämte, J., On-line prediction of mechanical pulp strenght and optical properties, SPCI, Blogna Italy 1992.
[95] Sjöström, E., Wood Chemistry - Fundamentals and Applications, Academic Press, New York 1993.
[96] Takano, T. and Tanaka, M., Phase matrix and cross sections for single scattering by circular cylinders; a comparison of ray optics and wave theory, Appl. Opt.**19**, 2781-2793 (1980).
[97] Tamminen J. Mätning och reglering av freeness i TMP-prosessen Diplom thesis. Åbo Akademi, Kemisk-tekniska fakulten. Turku (1987)
[98] Toivonen, H.T., and Tamminen, J., Minimax Robust LQ Control of a Thermomechanical Pulping Plant, Automatica, 26(2), 345-351(1990)
[99] Tornberg, J., Paavilainen, L., and Lohikoski, R., Mathematical analysis of fibre length distributions; applications to paper making, Proceedings of International Paper Physics Conference, 1991, 595-607.
[100] Toukonen J., Orkisz M., Wnek M., Saarinen K., Korendo Z. ARMADA – Advanced Rotating Machines Diagnostics Analysis tool for added service productivity, Proceedings of COMADEM2001 Confrerence,2001
[101] Vainio J., Eri säätöperiaatteiden soveltaminen hiertämön ohjauksessa. Diplom thesis, University of Oulu (1987)
[102] Weisberg S., Applied Linear Regression, Second edition, Whiley, New York (1985)
[103] Wold, H., A Study in the Analysis of Stationary Time Series, Almqvist & Wiksell, Stockholm, (1954).
[104] Wold, S., Antti, H., Lindgren, F., and Öhman, J., Orthogonal signal correction of Near Infra-red spectra, Chemometrics and Intelligent Laboratory Systems 44, 175-185 (1998).
[105] Wood J. R., Wild D. J., Karnis A., Stationwala M. I., Atack D., The Effect of Control Variables on Refining Zone Conditions and Pulp Properties Preprint International Mechanical Pulping Conference Toronto (1979)
[106] Ämmälä, A., Rautjärvi, H., Seppänen, A., and Niinimäki, J. Reliability of freeness measurement – errors in the analysis procedure, Proceedings of TAPPI Papermakers Conference and Trade Fair 147-158 (2000)

YHTEENVETO (FINNISH SUMMARY)

Hierteen laatu ja tehokas energian käyttö ovat avainasioita kaikissa kuumahierrelaitoksissa. Hierteen valmistusta haittaa kaksi eri tyyppistä häiriötä: hierrinterien hidas kuluminen ja raaka-aineen ominaisuuksien nopea vaihtelu. Molemmilla näistä on suuri vaikutus hierteen laatuun ellei niitä huomioida säädön avulla.

Tutkimuksen tarkoituksena oli ratkaista kuumahierreprosessin säätöongelma kehittämällä kalibrointimalleja ja -menetelmiä lähi-infrapuna tekniikkaa käyttävälle analysaattorille hierteen kosteuden ja laadun mittaamista varten sekä säätöjärjestelmä vaimentamaan raaka-ainevaihtelujen vaikutusta.

Työssä on kehitetty uusi säätöjärjestelmä raaka-ainevaihtelujen kompensointia varten. Se perustuu hierteen kosteusmittaukseen jauhimen puhallusputkessa ja siihen liittyvään adaptiiviseen säätöjärjestelmään joka muuttaa jauhimeen menevää laimennusvettä ja hakkeen syöttöruuvin pyörimisnopeutta. Järjestelmä vähentää huomattavasti energian ominais-kulutuksen ja jauhatusintensiteetin vaihteluja, jotka ovat tärkeimmät hierteen laatuun vaikuttavat jauhimen tilasuureet. Tämän seurauksena hierteen laatuvaihelut ovat vähentyneet, energiaa on voitu säästää, käytettävyys on parantunut ja tuotantoa on voitu lisätä. Tehdaskokeiden mukaan freeneksen, kuidunpituuden, repäisy- ja vetoindeksin vaihtelut ovat pienentyneet jopa 80 prosenttia. Järjestelmiä on asennettu jo yli yhdeksäänkymmeneen eripuolella maailmaa sijaitsevien tehtaiden hierrinlinjoihin.

Työssä on osoitettu, että lähi-infrapunatekniikalla voidaan mitata myös hierteen laatusuureita kuten freenestä, kuidunpituusjakaumaa sekä vetolujuutta. Koska analysaattori on asennettu heti jauhimen jälkeen laatutiedot saadaan mitattua aikaisempia menetelmiä nopeammin.

Kehitettyjen teoreettisten mallien avulla ymmärretään aikaisempaa paremmin lähi-infrapunasäteilyn ja puukuitujen välinen vuorovaikutus.

I

APPLICATION OF ADAPTIVE MODEL PREDICTIVE CONSISTENCY CONTROL IN TMP MILL

Saarinen K., 1990
Proceedings of the fifth European Conference in Mathematics in Industry (ECMI) conference, Lahti 1990. Heiliö M., ed. Kluwer
Academic Publisher, Dordrecht (1990). 335-339

II

ON THE CONTROL OF CHIP REFINING SYSTEMS

Hill J., Saarinen K., Stenros R., 1993
Pulp & Paper Canada 94:6 (1993). T 161- T 165

III

REFINER CONTROL EFFECTIVELY ACCOMPLISHED THROUGH ADAPTIVE CONTROL

Evans, R., Sutinen, R., and Saarinen, K., 1995
Pulp & Paper Canada 96:5 (1995). T 163-T 166

IV

DEVELOPMENTS IN SENSORS AND CONTROLS STRATEGIES FOR REFINERS

Evans R., Saarinen K., Sutinen R., 1992
CPPA 78th Annual Meeting, Montreal (1992)

V

A NOVEL CONTROL SYSTEM FOR REFINERS IN TMP PLANTS

Sutinen R., Saarinen K., 1992
SPCI, MILANO (1992)

VI

OPTIMAL QUALITY CONTROL OF TMP PLANTS

Leiviskä K., Sutinen R., Saarinen K., 1993
Preprint *International Mechanical Pulping Conference*, Oslo (1993)

https://www.researchgate.net/
publication/306943481_Optimal_quality_control_of_TMP-plants

VII

METHOD AND APPARATUS FOR DETERMINATION OF REFINER MECHANICAL PULP PROPERTIES

Saarinen K., 1996
United States Patent 5 491 340 (1996)

https://doi.org/10.1016/S0022-4073(98)00147-2

VIII

RAY OPTICS APPROXIMATION FOR GAUSSIAN RANDOM CYLINDERS

Muinonen K. and Saarinen K., 2000
Journal of Quantitative Spectroscopy and Radiative transfer 64(2000), 201-218

IX

LIGHT SCATTERING BY WOOD FIBERS

Saarinen K. and Muinonen K., 2001
Applied optics 40(28), (2001) 5064-5077

https://doi.org/10.1364/AO.40.005064